15. SITE 727[1]

Shipboard Scientific Party[2]

HOLE 727A

Date occupied: 24 September 1987

Date departed: 25 September 1987

Time on hole: 17 hr

Position: 17°46.096′N, 57°35.216′E

Water depth (sea level; corrected m, echo-sounding): 914.50

Water depth (rig floor; corrected m, echo-sounding): 925

Bottom felt (m, drill pipe): 921.50

Penetration (m): 182.40

Number of cores: 19

Total length of cored section (m): 182.20

Total core recovered (m): 188.40

Core recovery (%): 103.4

Oldest sediment cored:
Depth sub-bottom (m): 182.40
Nature: marly nannofossil ooze
Age: late Pliocene (NN18)
Measured velocity (km/s): —

HOLE 727B

Date occupied: 25 September 1987

Date departed: 25 September 1987

Time on hole: 4 hr, 30 min

Position: 17°46.096′N, 57°35.216′E

Water depth (sea level; corrected m, echo-sounding): 914.5

Water depth (rig floor; corrected m, echo-sounding): 925

Bottom felt (m, drill pipe): 918.8

Penetration (m): 27.10

Number of cores: 3

Total length of cored section (m): 27.10

Total core recovered (m): 27.95

Core recovery (%): 103.1

Oldest sediment cored:
Depth sub-bottom (m): 27.10
Nature: marly nannofossil ooze
Age: late Pleistocene (NN18)
Measured velocity (km/s): 1.52–1.61

Principal results: Site 727 is located in the northwestern Arabian Sea on the continental margin off the shore of Oman. The location corresponds to a second drilling target near the center of the pronounced oxygen-minimum zone (OMZ) that impinges on the margin underneath a zone of high biogenic productivity. We drilled Site 727 to complement the continuous and expanded sections of late Neogene to Holocene sediments previously recovered at Site 723, to trace the imprint of the OMZ through time, and to investigate diagenetic sedimentary processes.

Major findings at Site 727 include the identification of

1. a uniform lithology of marly nannofossil oozes ranging in age from latest Pliocene to Holocene;
2. calcareous nannofossils indicative of cold water and upwelling in the lower Pleistocene and only traces of opal in the uppermost Pliocene; and
3. complete sulfate depletion by 50 mbsf, replenished at depth by an unknown source. The sulfate increase is associated with a continuous downsection increase in alkalinity.

Our findings at Site 727 confirm many of the biotic and depositional trends observed at other sites on the Oman margin. However, the lack of laminated facies at Site 727, which lies at the same depth and covers the same time span as Site 723, poses questions about the character and spatial extent of the processes that led to the formation of laminated facies.

BACKGROUND AND OBJECTIVES

Site 727 is located in water depths of about 915 m at 17°46.096′N and 57°35.216′E on the continental margin of Oman. The location of Site 727 is shown in Figures 1 and 2, and its structural and depositional setting is shown in Figure 3. The site is located in the southern part of the slope basin, which is about 15 km wide here, and is bounded on the west by a faulted block and on the east by a basement ridge. Both basement features are thought to be ophiolite complexes.

The seismic reflection profiles of the basin sediments show numerous highly reflective layers in the upper 0.4 s that both onlap and drape the adjacent basement structures. The sediments are thickest in the center of the basin (more that 2000 m, based on sonobuoy data; Mountain and Prell, this volume) and thus form a syncline-shaped deposit (Fig. 3A). Along the strike of the basin (Fig. 3B), the shallow subsurface layers (0–0.4 s) dip gently to both the southwest and the northeast and are relatively conformable. In the deeper layers, some deformational, erosional, and slump-related structures are observed and appear to be associated with the basement peaks.

Site 727 was located within a zone of continuous westward dipping reflectors (Figure 3A) on the seaward margin of the slope basin. The preliminary correlation of seismic reflectors within the basin indicates that the average accumulation rates are highest in the southern part of the basin near the location of Site 723. They were expected to be somewhat lower at Site 727 because it is not in the center of the basin (Fig. 3A).

Specific objectives for drilling at Site 727 were

1. to obtain a high-resolution record of the sediments associated with the near-coastal zone of the monsoonal upwelling system, in order to establish the changes in timing and intensity of the monsoon; and
2. to provide a deep-water section in the depth transect of sites across the Oman margin that can be used to examine the organic-rich sedimentary facies of the margin and establish their relationship to the OMZ and its spatial variation through time.

[1] Prell, W. L., Niitsuma, N., et al., 1989. *Proc. ODP, Init. Repts.*, 117: College Station, TX (Ocean Drilling Program).

[2] Shipboard Scientific Party is as given in the list of Participants preceding the contents.

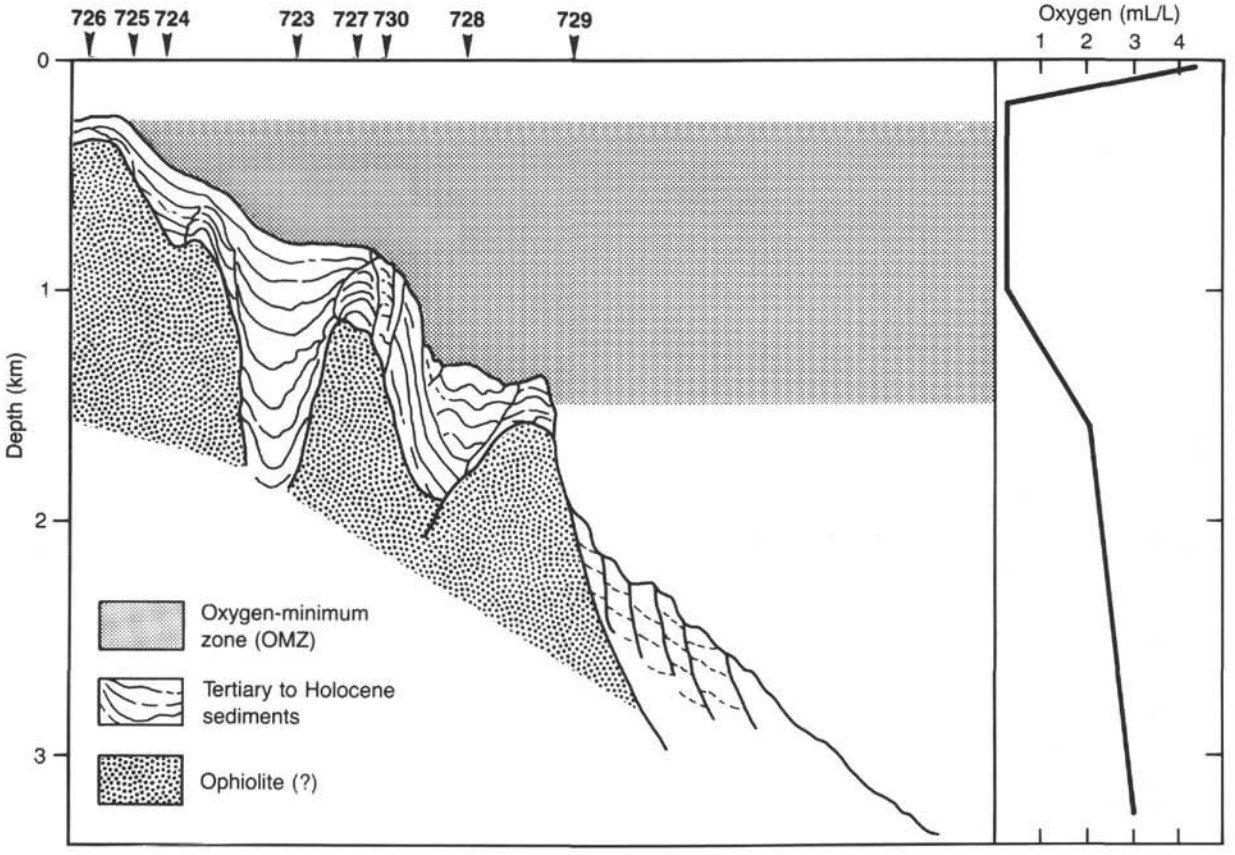

Figure 1. Structure of the Oman margin and the oxygen-minimum zone (OMZ). The schematic profile shows the series of basement ophiolite blocks and the sedimentary basins between them. The concentration of oxygen in the water column (RC2704, unpubl. data) defines the depth range of the OMZ and where it impinges on the margin.

OPERATIONS

The ship departed Site 726 at 0830 hr on 24 September 1987 and surveyed Site 727 with the seismic gear streamed before the site was occupied and drilling operations began. We dropped the beacon in water depths of 914 m upon passing the site for the second time and retrieved the seismic gear. The ship attained dynamic positioning mode by 1230 hr on 24 September. The exact location of Site 727 was obtained from Global Positioning System (GPS) as 17°46.096′N and 57°35.216′E (Fig. 4).

The first of 10 APC cores was shot at 1430 hr, followed by 9 XCB cores to a total depth of 182.2 mbsf in Hole 727A. We switched to the XCB mode after reaching 95.4 mbsf due to a pull-out force of 110,000 lbs upon retrieving Core 117-727A-10H. Recovery in the section cored by the APC was 104%. Recovery with the XCB continued to be excellent down to total depth and averaged 102% in calcareous oozes and clayey silts, even though gas expansion was less severe than at other sites. *In-situ* pore-water samples were collected after Cores 117-727A-9H and -10X (Table 1).

At 0030 hr on 25 September, the hole was displaced with mud and the string was pulled after we reached target depth in Hole 727A. Without offsetting the rig, the bit was positioned to shoot the mud line of Hole 727B, which consists of three APC cores from 0 to 27.1 mbsf, an interval which was cored from 0215 to 0345 hr on 25 September 1987. These cores had 103% recovery. Operations at Site 727 were finished after pulling the string, and the ship set out to survey Sites 728 and 729 by 0600 hr on 25 September 1987.

LITHOSTRATIGRAPHY

Lithologic Units

Sediments recovered from Site 727 range from Holocene to late Pliocene in age. Visual core descriptions, smear slide analyses, and calcium carbonate contents indicate a uniform lithology. A single lithologic unit, consisting of calcitic marly nannofossil ooze to calcitic marly calcareous ooze, has been assigned to the entire sedimentary column (Fig. 5).

Unit I (Depth: Hole 727A, 0–182.4 mbsf; Hole 727B, 0–27.1 mbsf; Age: late Pliocene to Pleistocene)

Cores 117-727B-1H through -19X; Cores 117-727B-1H to -3H.

Lithologic Unit I consists of sediments which grade between calcitic marly nannofossil ooze and calcitic marly calcareous ooze. The sediments range in color from olive (5Y 4/3) to olive gray (5Y 4/2, 5/2), and dark olive gray (5Y 3/2).

Smear slide analyses indicate that the sediment in Unit I is dominated by biogenic carbonate. The carbonate is composed primarily of nannofossils (as much as 55%), but it also contains as much as 20% foraminifers. The nonbiogenic component is dominated by clay (15%–35%) and detrital calcite (15%–40%). Other minerals, usually comprising less than 10% of the sediment, include quartz, trace amounts of dolomite, and opaque minerals (Table 2). Given the resolution of these preliminary data, the mineralogical components show no significant variations within the sedimentary column.

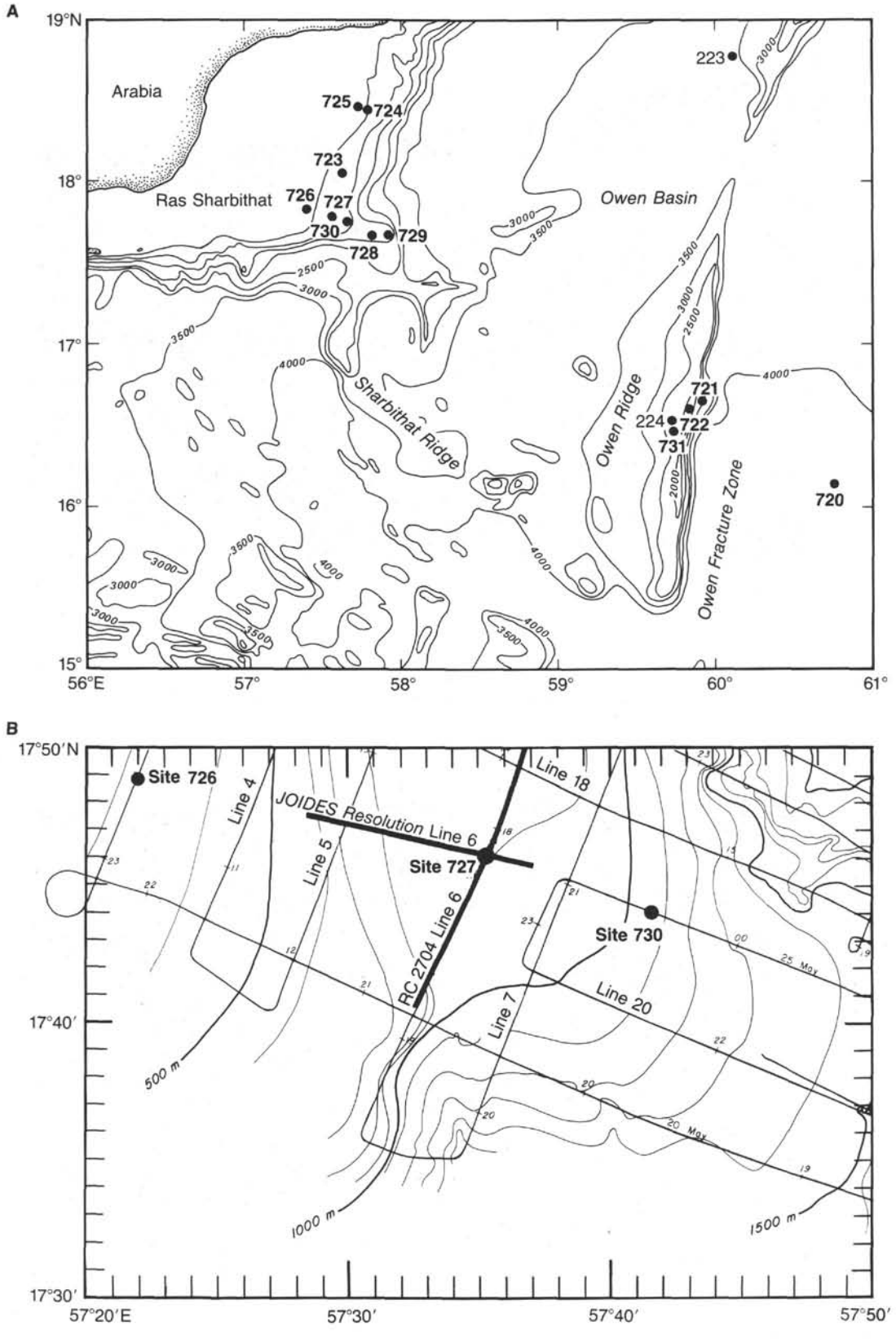

Figure 2. A. Bathymetry of the Oman margin and the location of Site 727. B. The detailed location of Site 727 and the seismic profiles shown in Figure 3. Bathymetric data are from the site survey (RC2704, 1986).

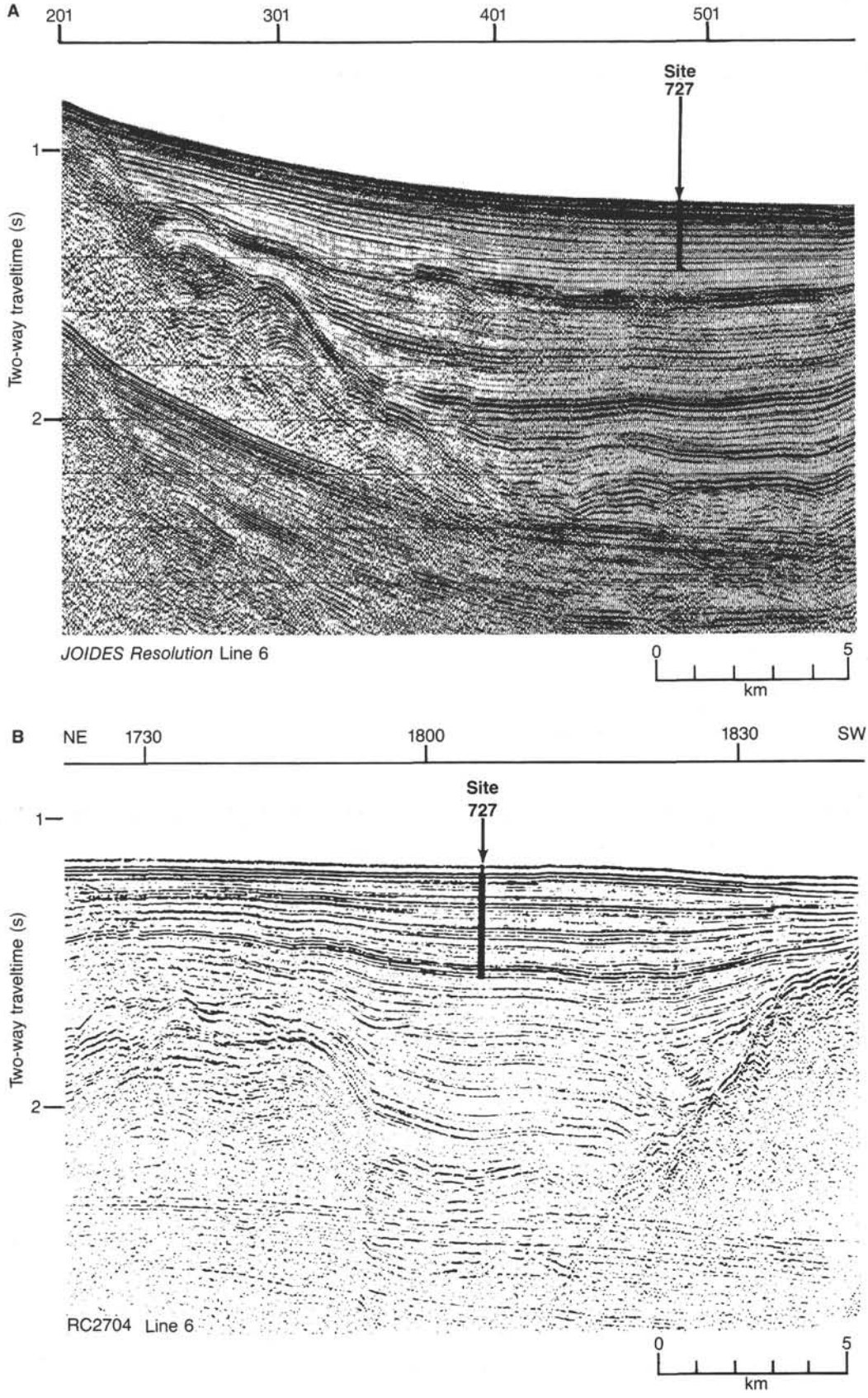

Figure 3. A. Single-channel-seismic (SCS) reflection profiles showing the structural and depositional setting of Site 727. Line 18 is perpendicular to the trend of the basin and shows the bounding basement blocks and the synclinal-shaped sediment fill. The relative position of Site 727 is projected. B. Line 6 is along the strike of the basin and shows the sediment thickness decreasing to the northeast and southwest.

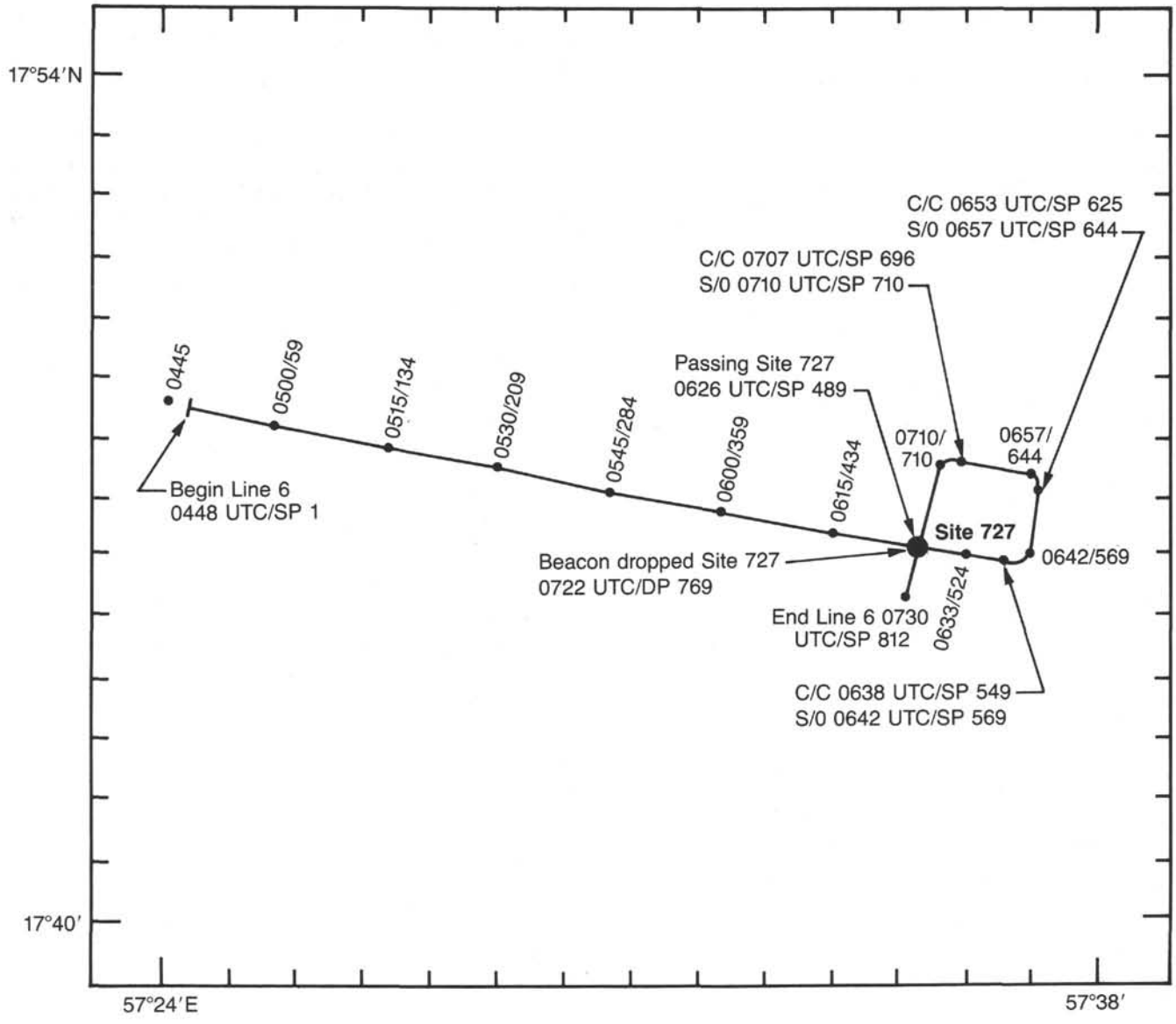

Figure 4. Track line of *JOIDES Resolution* during the survey of Site 727.

The calcium carbonate content (Table 3 and Fig. 6) ranges from 46% to 70% and averages 58%. Foraminifer and nannofossil data (see "Biostratigraphy" section, this chapter) indicate that carbonate preservation is good from the top of the section through Core 117-727A-10H (0–94 mbsf) and moderate from Cores 117-727A-10H to -19X (94–182 mbsf). The organic carbon content (Table 3 and Fig. 6) ranges from 0.80% to 4.96%, with the highest values occurring from Cores 117-727A-14X to -16X (126–165 mbsf).

Deviations from the major lithology encompass a total sediment thickness of less than 1 m and are as follows: (1) greenish gray (5GY 5/1) nannofossil-rich calcitic clayey sand (Sample 117-727A-14X-2, 120–121 cm), and (2) dark olive gray (5Y 3/2) nannofossil-rich calcitic silty clay (Samples 117-727B-3H-2, 28–41 cm; 117-727B-3H-2, 93–103 cm; and 117-727B-3H-4, 58–88 cm).

Discussion

The uniform lithology at Site 727 indicates that this site has been under the influence of a relatively constant (dominantly hemipelagic) depositional regime since the late Pliocene. Site 727 occupies the same sedimentary basin as Site 723 (located 28 km north of Site 727). By comparison, Sites 727 and 723 have similar lithologies from the upper Pliocene through the Pleistocene with the exception that no laminated sediments were identified at Site 727. Preliminary estimates, based largely on sediment accumulation rates and benthic foraminifer data, indicate that the two sites were at similar paleodepths from the late Pliocene through the early Pleistocene. During this interval, silica-rich laminated sediments with high organic carbon content were deposited at Site 723; sediments deposited at Site 727, on the other hand, contained only trace amounts of biogenic silica, had high organic carbon contents (up to 5%), and were not laminated. These observations suggest small-scale horizontal heterogeneity in the environmental and depositional conditions within the OMZ.

Site 724, located 70 km north-northwest of Site 727 in the same sedimentary basin, occupied a much shallower paleodepth throughout the Pliocene and Pleistocene. Laminae at Site 724, however, occur only below the Pliocene-Pleistocene boundary,

Table 1. Coring summary, Site 727.

Core no.	Date (Sept. 1987)	Time	Depth (mbsf)	Cored (m)	Recovered (m)	Recovery (%)
117-727A-						
1H	24	1505	0–9.5	9.5	9.57	101.0
2H	24	1520	9.5–18.9	9.4	9.19	97.7
3H	24	1540	18.9–28.4	9.5	9.95	105.0
4H	24	1600	28.4–37.8	9.4	9.88	105.0
5H	24	1715	37.8–47.3	9.5	9.85	103.0
6H	24	1735	47.3–56.8	9.5	9.98	105.0
7H	24	1755	56.8–66.4	9.6	10.03	104.5
8H	24	1815	66.4–76.1	9.7	10.18	104.9
9H	24	1835	76.1–85.8	9.7	10.20	105.1
10H	24	1900	85.8–95.4	9.6	10.45	108.8
11X	24	2045	95.4–105.0	9.6	9.99	104.0
12X	24	2110	105.0–114.6	9.6	9.52	99.1
13X	24	2130	114.6–124.0	9.4	10.14	107.9
14X	24	2150	124.0–133.7	9.7	10.67	110.0
15X	24	2210	133.9–143.6	9.7	9.80	101.0
16X	24	2240	143.6–153.3	9.7	9.73	100.0
17X	24	2300	153.3–163.0	9.7	9.87	102.0
18X	24	2320	163.0–172.7	9.7	9.95	102.0
19X	24	2350	172.7–182.4	9.7	9.45	97.4
				182.2	188.40	
117-727B-						
1H	25	0230	0–8.2	8.2	8.15	99.4
2H	25	0250	8.2–17.6	9.4	9.91	105.0
3H	25	0315	17.6–27.1	9.5	9.89	104.0
				27.1	27.95	

suggesting the possibility of both temporal and vertical heterogeneity in the conditions necessary for the formation of laminated sediments. Detailed stratigraphic, paleontologic, and sedimentologic studies are needed to map the paleodistribution of laminated sediments accurately and to evaluate the environmental conditions under which they formed.

The continuous, uniform nature of Site 727 sediments are ideal for the development of high-resolution faunal, oxygen-isotope, and carbonate records. A comparison of these records with similar records from the Owen Ridge will help to determine the differences between the nearshore and open-marine monsoonal upwelling regimes.

BIOSTRATIGRAPHY

Introduction

Site 727 is located in water depths of 914 m. The Pleistocene-Pliocene boundary was recognized at about 150 mbsf, based on calcareous nannofossil data (Fig. 7). A plot of faunal datum levels and paleomagnetic reversals vs. depth below the seafloor is presented in Figure 8; for a detailed listing of these data points see Table 4.

Siliceous microfossils at this site are absent down to 143.6 mbsf. Below this level only rare fragments are found. Calcareous microfossils (planktonic and benthic foraminifers and nannofossils) are present throughout Hole 727A. Preservation is moderate to good and the abundance of planktonic foraminifers and nannofossils is high. Benthic foraminifers are rare to few in the upper 47.3 m, but they become more abundant below this level.

Planktonic Foraminifers

The drilled sequence of Site 727 contains highly diverse planktonic foraminiferal assemblages. All core-catcher samples studied yielded abundant specimens, except for the lowermost Core 117-727A-19X. Preservation of the tests is moderate to good. The presence of *Globorotalia truncatulinoides* shows that the age of the sediments throughout the entire sequence is Pleistocene, except for the lowermost Sample 117-727A-19X, CC (182.4 mbsf), which may be late Pliocene in age.

Benthic Foraminifers

We studied the benthic foraminifer fauna of Site 727 in the core-catcher samples of Hole 727A. Abundance varied from few to rare in the upper five samples (9.5–47.3 mbsf). Benthic foraminifers are abundant in the next three samples (56.8–76.1 mbsf) and become common further downhole (below 85.8 mbsf). Preservation is good to moderate. The planktonic/benthic (P/B) ratio is high throughout the sequence studied.

Benthic foraminifer fauna at this site are characterized by a high relative abundance of uvigerinoids, especially *Uvigerina peregrina.* Additional species that commonly occur throughout the sequence are *Bolivina ordinaria, Cassidulina carinata,* and *Hyalinea baltica.*

The stability in the faunal composition and the high P/B ratio indicate no major variations in the water depth and suggest that the present location in the upper middle bathyal zone already was established in the late Pliocene.

Calcareous Nannofossils

Hole 727A

A high abundance and moderate to good preservation characterize the calcareous nannofossil assemblages from Hole 727A. However, there is comparatively low species diversity. The cored sediments range in age from Holocene to latest Pliocene.

The nannofossil assemblages in sediments down to 23.08 mbsf are composed predominantly of such placoliths as *Gephyrocapsa oceanica, G. caribbeanica, G. parallela,* and *Emiliania huxleyi.* Therefore, these sediments are assigned to Zone NN21 (Holocene to Pleistocene). Underlying sediments as far down as 41.98 mbsf contain neither *E. huxleyi* nor *Pseudoemiliania lacunosa* and are referred to Zone NN20 (Pleistocene). The presence of *P. lacunosa* and the absence of discoasters in sediments from 42 to 179.90 mbsf place this section in Zone NN19.

The Pleistocene/Pliocene boundary is placed between Samples 117-727A-16X-3, 118–119 cm, and 117-727A-16X-5, 114–115 cm (147.78–150.74 mbsf). The top of *Discoaster brouweri* is between 179.90 and 182.40 mbsf. We assigned sediments below this level down to the bottom of the hole to Zone NN18 (upper Pliocene).

As has been the case at previous sites, nannofossil species such as *Ceratolithus cristatus, Rhabdosphaera clavigera,* and *Oolithotus antillarum* are absent in this hole. *Pseudoemiliania lacunosa* is also rare throughout Zones NN19 and NN18. It is noteworthy that we recognized *Coccolithus pelagicus,* which is a typical cold-water species, in sediments below 163.0 mbsf.

Hole 727B

A total of 27.95 m of sediments was recovered from the second hole at Site 727. Sediments from the mud line to 17.6 mbsf contain *Emiliania huxleyi* and belong to Zone NN21 (Holocene to Pleistocene). We assigned underlying sediments down to the bottom of this hole to Zone NN20 (Pleistocene) because they contain neither *E. huxleyi* nor *P. lacunosa.*

Radiolarians

Most of the recovered material at Site 727 is barren of radiolarians. Rare, non-age-diagnostic fragments only were found in Samples 117-727A-15X, CC (143.6 mbsf), and 117-727A-17X, CC, through -19X, CC (163.0–182.4 mbsf).

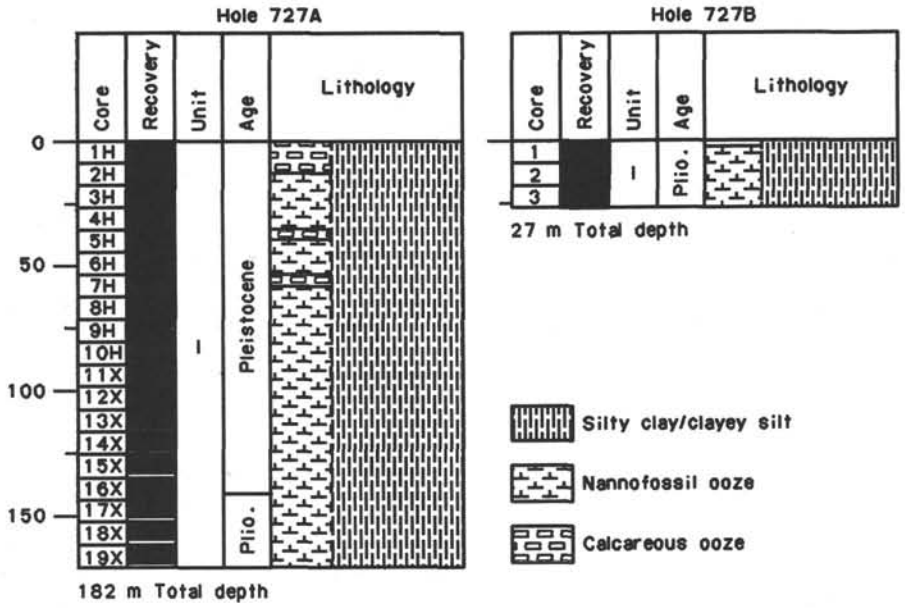

Figure 5. Lithostratigraphic summary columns, Site 727. Black bars represent recovery in Holes 727A and 727B.

Table 2. Smear slide summary, Site 727.

Component	Range	Average
Nannofossils	15%–55%	36%
Clay	15%–35%	26%
Detrital calcite	15%–40%	23%
Foraminifers	00%–20%	7%
Other minerals[a]	03%–12%	8%

[a] Primarily quartz with trace amounts of dolomite and opaque minerals.

Paleoenvironmental Implications

The high P/B ratio suggests that no major changes in the water depth at this site has occurred since the late Pliocene.

PALEOMAGNETISM

Introduction

Sediments recovered at Site 727 were homogeneous and comprised foraminifer-bearing marly nannofossil ooze and calcareous clayey silt. One discrete paleomagnetic sample per section was obtained from Hole 727A, and the magnetic susceptibility of whole-core sections was measured in both holes.

Magnetostratigraphy

We measured the natural remanent magnetization (NRM) of discrete samples with the Molspin Minispin spinner magnetometer. Magnetic cleaning was accomplished with the Schonstedt Alternating Field (AF) Demagnetizer. We selected peak AF demagnetization fields of 5 or 10 mT, depending on the initial intensity. Stepwise demagnetization of a sample from the uppermost part (117-727A-1H-6, 115–117 cm) is shown in Figure 9. As indicated by this example, samples from the upper 70 m interval had relatively high magnetic intensities ranging from 0.5 to 5.9 mA/m and high stability (median destructive field about 20 mT). Below ~100 mbsf, magnetic intensity was generally <0.5 mA/m. The samples from this interval were demagnetized at 5 mT peak AF. The overall logarithmic mean of the magnetic intensity is 0.6 mA/m.

Figure 10 shows downhole plots of magnetic directions and intensities. These plots were obtained after filtering all data with circular standard deviations (CSD) >40°. As also illustrated in the histogram in Figure 11, the inclination values of normal and reversed polarity show a rather asymmetric distribution; while positive inclinations are distributed around the value expected from the geocentric axial dipole field (32.7°), negative inclinations mostly range from −30° to 0°. The smaller absolute inclination values of reversed polarity may be explained by the insufficient removal of secondary magnetic overprints.

The inclination plot in Figure 10 shows that Hole 727A sediment is clearly divided into at least five polarity intervals. We assigned the normal polarity zone between 0 and about 80 mbsf to the Brunhes Chronozone (C1), and the interval below 80 mbsf to the Matuyama Chronozone. The two normal polarity zones, ranging from 96 to 105 mbsf and from about 160 mbsf to the bottom of the hole, can be assigned to the Jaramillo and Olduvai Subchronozones (C1r-1 and C2), respectively (Table 5). These assignments are concordant with the biostratigraphic datums of calcareous nannoplankton (see "Biostratigraphy" section, this chapter).

Magnetic Susceptibility

The magnetic susceptibility of Holes 727A and 727B were measured with the Bartington Susceptibility Meter (Model MS1) and a whole-core, pass-through sensor coil of 80-mm inner diameter (Model MS2C) at the 0.1 sensitivity and low-frequency (0.47 kHz) settings. All measurements were made at 10-cm intervals. The excellent recovery and core quality obtained at Site 727 resulted in one of the highest quality susceptibility records yet produced from Leg 117 drilling on the Oman margin.

The susceptibility values observed at Site 727 were similar in magnitude to those measured at Site 723. The approximate range of values is 30×10^{-6} to 100×10^{-6} volume SI units (Fig. 12). On average, these values are considerably lower than those values obtained from the other Oman margin sites (i.e., 724, 725, and 726). Since Sites 723 and 727 have the two highest accumulation rates of the margin sites (~180 and ~95 m/m.y., respec-

Table 3. Inorganic carbon, organic carbon, and carbonate, Site 727.

Core, section, interval (cm)	Depth (mbsf)	Total carbon (%)	Inorganic carbon (%)	Organic carbon (%)	$CaCO_3$ (%)
117-727A-					
1H-2, 100-102	2.50	10.05	6.64	3.41	55.3
1H-4, 100-102	5.50	6.71			55.9
1H-6, 100-102	8.50	7.79			64.9
2H-2, 50-52	11.50	8.36	6.81	1.55	56.7
2H-4, 50-52	14.50	6.67			55.6
3H-2, 100-102	21.40	10.67	7.39	3.28	61.6
3H-4, 78-80	24.18	6.88			57.3
3H-4, 119-120	24.59	8.84	6.82	2.02	56.8
3H-6, 34-36	26.74	7.30			60.8
4H-2, 6-8	29.96	8.39			69.9
4H-4, 6-8	32.96	7.22			60.1
4H-6, 6-8	35.96	8.24			68.6
5H-2, 71-73	40.01	7.83	7.03	0.80	58.6
5H-4, 32-34	42.62	7.35			61.2
6H-2, 50-52	49.30	8.70	7.13	1.57	59.4
6H-4, 111-113	52.91	8.01			66.7
6H-4, 119-120	52.99	9.21	8.12	1.09	67.6
6H-6, 8-10	54.88	7.98			66.5
6H-6, 50-52	55.30	5.76			48.0
7H-2, 123-125	59.53	8.14	6.54	1.60	54.5
7H-4, 8-10	61.38	6.20			51.7
7H-6, 8-10	64.38	7.25			60.4
8H-2, 24-26	68.14	10.26	8.04	2.22	67.0
8H-4, 40-42	71.30	7.52			62.6
8H-6, 8-10	73.98	7.48			62.3
9H-3, 27-29	79.37	7.57	6.65	0.92	55.4
9H-5, 119-120	83.29	8.19	7.09	1.10	59.1
9H-6, 63-65	84.23	6.90			57.5
10H-3, 80-82	88.32	9.93	6.68	3.25	55.6
10H-5, 90-92	91.42	7.76			64.6
10H-7, 88-90	94.40	7.16			59.6
11X-2, 76-78	97.66	7.97	6.27	1.70	52.2
11X-4, 25-27	100.15	6.73			56.1
11X-6, 85-87	103.75	7.20			60.0
12X-2, 98-100	107.48	9.73	7.59	2.14	63.2
12X-4, 98-100	110.48	7.53			62.7
12X-4, 144-145	110.94	10.43	7.77	2.66	64.7
12X-6, 98-100	113.48	7.24			60.3
13X-2, 0-1	116.10	9.24	7.12	2.12	59.3
13X-2, 93-95	117.03	8.39	6.52	1.87	54.3
13X-4, 102-104	120.12	6.78			56.5
13X-6, 80-82	122.90	7.40			61.6
14X-2, 98-100	126.48	10.63	7.16	3.47	59.6
14X-4, 133-135	129.83	6.31			52.6
14X-4, 149-150	129.99	9.59	5.95	3.64	49.6
14X-7, 18-20	133.18	7.18			59.8
15X-2, 28-30	135.68	11.16	6.93	4.23	57.7
15X-4, 17-19	138.57	6.35			52.9
15X-5, 119-120	141.09	12.23	7.27	4.96	60.6
15X-6, 58-60	141.98	7.24			60.3
16X-2, 80-82	145.90	10.43	6.37	4.06	53.1
16X-4, 60-62	148.70	6.30			52.5
16X-4, 149-150	149.59	8.41	5.76	2.65	48.0
16X-6, 114-116	152.24	5.53			46.1
17X-2, 94-96	155.74	8.74	5.87	2.87	48.9
17X-4, 95-97	158.75	6.39			53.2
17X-5, 0-1	159.30	10.70	6.63	4.07	55.2
17X-6, 120-122	162.00	5.50			45.8
18X-2, 84-86	165.34	10.74	6.92	3.82	57.6
18X-3, 119-120	167.19	9.18	8.13	1.05	67.7
18X-4, 104-106	168.54	7.77			64.7
18X-6, 98-100	171.48	7.68			64.0
19X-1, 135-137	174.05	10.49	7.64	2.85	63.6
19X-3, 0-1	175.70	9.86	7.91	1.95	65.9
19X-3, 128-130	176.98	7.39			61.6
19X-5, 95-97	179.65	6.34			52.8

tively), the lower susceptibility values are most probably attributable to dilution by nonmagnetic components.

The practical utility of susceptibility as a high-resolution stratigraphic tool could be demonstrated at Site 727. The data for the first 10 APC cores of Hole 727A, which were plotted while the hole was being drilled in the XCB mode, indicated that the mud line was missed and that several meters of sediment were not recovered. Since an objective of this site was to obtain a high-resolution upper Neogene sequence, a decision was made to spud-in a second hole so that the uppermost sediments could be recored. The susceptibility data of the three 727B APC cores indicated that ~4 meters of surficial sediment were not recovered at Hole 727A (Fig. 13).

Detailed correlations of Site 727 with other Oman margin sites and with the Owen Ridge sites are clearly apparent when the data are plotted at approximately equivalent time intervals. Figure 14 shows the susceptibility-derived correlations between Holes 723B and 727A from the Oman margin and Hole 722B from the Owen Ridge for the Brunhes Chronozone (0.73 Ma). No detailed correlations were possible between Site 727 and other margin sites below the Brunhes Chronozone since a susceptibility record of equal quality to Site 727 was not available at the time of writing; however, correlations exist between Site 727 and other Owen Ridge sites beyond the Jaramillo Subchronozone (>0.98 Ma). Detailed interhole correlations based on these susceptibility data and distinct lithologic marker layers are presented in the "Interhole Correlation" section of this chapter.

ACCUMULATION RATES

Magneto- and biostratigraphic data are used to determine sedimentation rates at Site 727 for the last 1.9 m.y. (Table 4). Sedimentation rates are calculated between nannofossil datums whose ages are based on oxygen-isotope stratigraphy (Niitsuma, unpublished data) and Berggren et al. (1985a, 1985b); this information is given in Table 4 and Figure 15. Rates vary between 60 and 133 m/m.y., with a mean of 95 m/m.y. for the last 1.9 m.y.

Much of the variation in sedimentation rate at the top of Hole 727A (Fig. 16) is based on the location and age of the LAD of *Pseudoemiliania lacunosa*. We assigned an age of 0.49 m.y. to this datum based on the oxygen-isotope data in nearby Site 723 (Niitsuma, unpublished data). However, if an age close to 0.40 m.y. is used, there is little variation in the mean sedimentation rate of 105 m/m.y. for the top 120 m of Site 727.

Since sediments are relatively homogeneous at Site 727 (see "Lithostratigraphy" section, this chapter), large variations in mean sedimentation rate are unexpected. Post-cruise analysis of the stratigraphic datums is necessary to determine whether the variations in mean sedimentation rate based on the present age model are correct.

In comparison with nearby Site 723, sediments accumulated at Site 727 at almost one half the rate of Site 723. These differences are attributed to the differences in tectonic setting of the two sites: Site 727 is near the edge and Site 723 is in the center of the upper slope basin.

The mass accumulation rates of calcium carbonate, organic carbon, and noncarbonate sediment components are calculated from average values between the nannoplankton datum levels (Table 6). During the Pleistocene to late Pliocene, sediments accumulated at Site 727 at rates between 7 and 13 $g/cm^2/k.y.$ These values are comparable with those observed at Site 725 to the north. The high rates of organic carbon accumulation near the Pliocene/Pleistocene boundary (Table 6) are associated with sediments containing more biogenic silica (see "Lithostratigraphy" section, this chapter), an association which is observed at other Oman margin sites.

Based on smear slide analyses, sediments at Site 727 and at all other Oman margin sites contain abundant detrital calcite. Therefore, the accumulation of calcium carbonate in Figure 16 contains both detrital and pelagic components. Until the relative contributions of these components are determined, the accumulation of calcite cannot be used to infer changes in biogenic calcium carbonate production in surface waters.

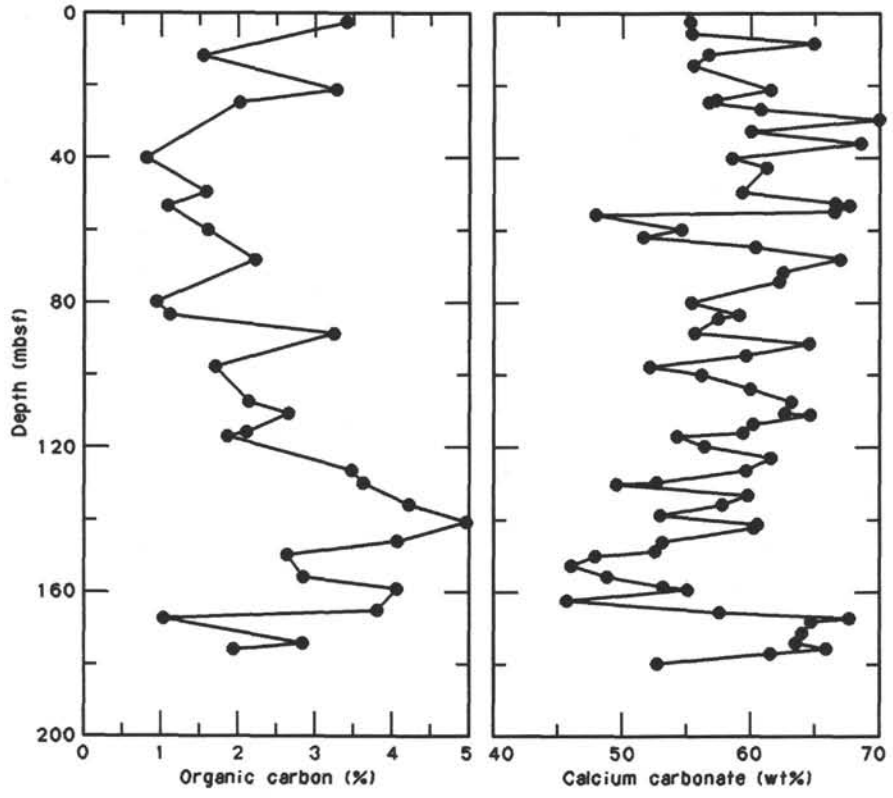

Figure 6. Calcium carbonate and organic carbon content, Site 727. The highest values of organic carbon occur from 126 to 165 mbsf.

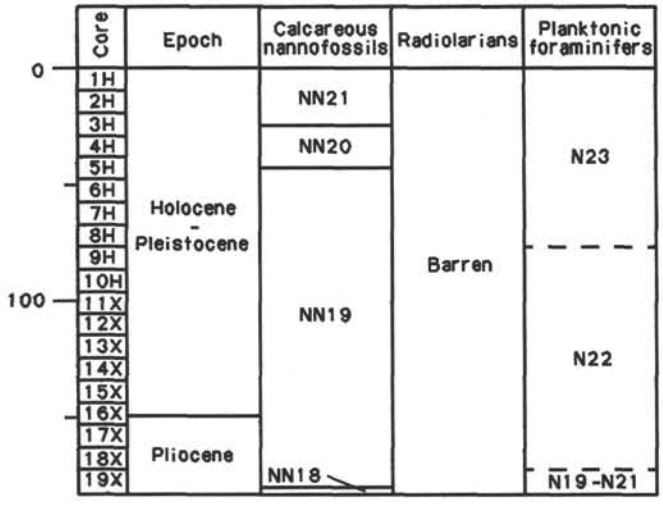

Figure 7. Correlation of planktonic microfossil zones in Hole 727A.

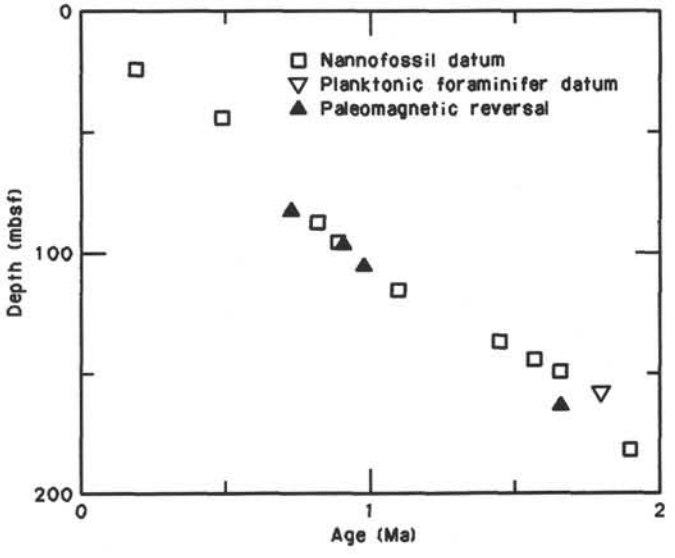

Figure 8. Age-depth plot for Hole 727A. For a detailed listing of events, see Table 4.

PHYSICAL PROPERTIES

Introduction

The problems we experienced at Sites 723, 724, and 725 in measuring the physical properties of sediments disturbed by gas-induced expansion were also encountered at Site 727. Physical properties measured on discrete samples included index properties (wet-bulk density, porosity, water content, and grain density), thermal conductivity, and vane shear strength (Table 7). We could not measure compressional-wave velocities with the Hamilton Frame Velocimeter because the sediments were not sufficiently indurated.

The GRAPE and *P*-wave logger were used to measure continuous wet-bulk density and compressional-wave velocity profiles in core sections longer than 80 cm. Acquisition of reliable data with the GRAPE and *P*-wave logging systems was limited to sediments recovered from depths <65 mbsf.

Table 4. Biostratigraphic listing of faunal events and paleomagnetic reversals for Hole 727A.

	Event	Core, section, interval (cm)	Depth (mbsf)	Age (Ma)	Source of age
B	*Emiliania huxleyi*	117-727A-3H-3, 118-119	23.08	0.19	3
		117-727A-3H-5, 118-119	26.08		
T	*Pseudoemiliania lacunosa*	117-727A-5H-3, 118-119	41.98	0.49	3
		117-727A-5H-5, 118-119	44.98		
	Brunhes/Matuyama	117-727A-9H-4, 115-117	81.75	0.73	6
		117-727A-9H-5, 115-117	83.25		
T	*Reticulofenestra* sp. A	117-727A-9H, CC	85.80	0.82	3
		117-727A-10H-3, 118-119	88.70		
B	*Gephyrocapsa parallela*	117-727A-10H-7, 118-119	94.70	[a]0.89	4
		117-727A-10H, CC			
T	Jaramillo	117-727A-10H-8, 85-87	95.87	0.91	6
		117-727A-11X-1, 101-103	96.41		
B	Jaramillo	117-727A-11X-6, 124-126	104.14	0.98	6
		117-727A-12X-1, 101-103	106.01		
T	*Gephyrocapsa* "large"[b]	117-727A-12X, CC	114.60	[a]1.10	4
		117-727A-13X-1, 118-119	115.78		
T	*Helicosphaera sellii*	117-727A-14X-1, 118-119	125.18	[c]	
		117-727A-14X-3, 114-115	128.14		
T	*Calcidiscus macintyrei*	117-727A-15X-1, 106-107	134.96	1.45	6
		117-727A-15X-3, 116-117	138.06		
B	*Gephyrocapsa oceanica*	117-727A-15X, CC	143.60	[a]1.57	4
		117-727A-16X-1, 118-119	144.78		
B	*Gephyrocapsa caribbeanica*	117-727A-16X-3, 118-119	147.78	[d]1.66	4, 8
		117-727A-16X-5, 114-115	150.74		
T	*Globigerinoides extremus*	117-727A-16X, CC	153.30	[e]1.8	6
		117-727A-17X, CC	163.00		
T	Olduvai	117-727A-17X-6, 126-128	162.06	1.66	6
		117-727A-18X-1, 94-96	163.94		
T	*Discoaster brouweri*	117-727A-19X-5, 120-121	179.90	1.9	6
		117-727A-19X, CC	182.40		

Note: T = upper limit of event and B = lower limit. Sources of ages are: 3 = oxygen isotope data for Site 723 (N. Niitsuma, unpubl. data); 4 = Takayama and Sato, 1987; 6 = Berggren et al., 1985b; and 8 = Sato et al., in press.

[a] North Atlantic data.

[b] Long axis greater than 6 μm.

[c] No good published age; event appears to be diachronous.

[d] North Atlantic age consistent with Italian-type section.

[e] *G. obliquus extremus* cited in Berggren et al., 1985b.

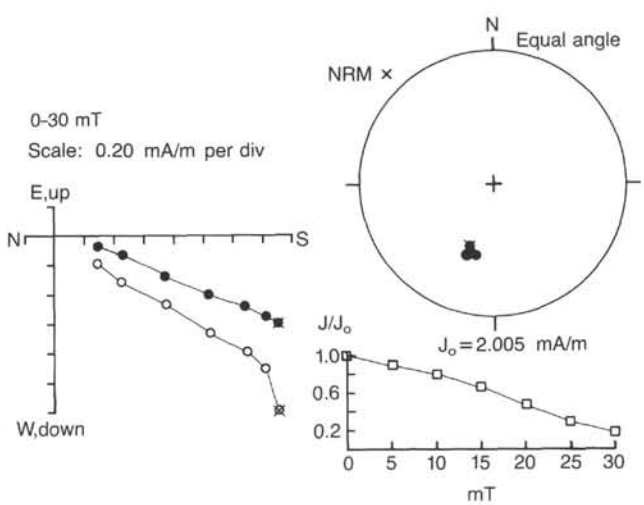

Figure 9. Result of stepwise alternating field (AF) demagnetization for Sample 117-727A-1H-6, 115-117 cm, from 0 to 30 mT.

Index Properties

The uniform lithology of marly nannofossil ooze at Site 727 is characterized by a gradual change in index properties with increasing burial depth. Porosity and water content decrease from 66% and 43%, respectively, at the seafloor to values of 56% and 33% at 180 mbsf (Fig. 17). Grain density shows little variation about an average value of 2.59 g/cm^3; as a consequence, decreasing water content is responsible for an increase in wet-bulk density from 1.58 g/cm^3 at the seafloor to 1.80 g/cm^3 at 180 mbsf (Fig. 17).

The most prominent feature of the index properties profiles is the sharp reduction in the variability of water content, porosity, and wet-bulk density which occurs at 88 mbsf. This depth roughly coincides with the depth at which foraminifer abundance decreases, suggesting that greater water content variability above 88 mbsf is a consequence of textural variation. The coarse grain size of intervals enriched in foraminifers may cause those layers to exhibit lower water content and higher bulk density than adjacent finer-grained sediment.

In addition to the change in the uniformity of the index property profiles at 88 mbsf, there is a 6% increase in porosity (56% to 62%) and a 0.13 g/cm^3 decrease in wet-bulk density (1.80 to 1.67 g/cm^3) over the interval from 84 to 88 mbsf (Fig. 17). These porosity and bulk density changes reflect an increase in average organic carbon content from 1.10% to 3.25% (see "Organic Geochemistry" section, this chapter). Between 88 mbsf and the bottom of Hole 727A (182.4 mbsf), porosity decreases from 62% to 56%, water content decreases from 38% to 33%, and wet-bulk density increases from 1.67 to 1.75 g/cm^3.

These trends are reversed in the interval between 126 and 165 mbsf, coinciding with an increase in organic carbon content. In this depth range there is a slight decrease (0.05 g/cm^3) in wet-bulk density and an increase (3%) in porosity (Fig. 17). The lowest grain densities (2.43 to 2.46 g/cm^3) occur between 138 to 146 mbsf and correspond to a peak in the organic carbon abundance (4.06%–4.96%). Below 165 mbsf a slight increase in grain density, decreases in porosity and water content, and an increase in wet-bulk density reflect decreasing abundance of organic matter and sediment dewatering controlled by increasing overburden pressure.

GRAPE and *P*-Wave Logs

Determination of wet-bulk density by the GRAPE and compressional-wave velocity with the *P*-wave logger was limited by sediment expansion. Continuous GRAPE data were obtained through Core 117-727A-10H (95.4 mbsf); however, below 65 mbsf the quality of the data decreases as a consequence of expansion-related fractures. Between 65 and 95 mbsf the character of the GRAPE records is retained, but GRAPE estimates of wet-bulk density are less than densities determined for discrete samples and there is more high-frequency noise in the data. The GRAPE records display a cyclic variation similar to that observed at Sites 723 and 724. The thickness of the cycles at Site 727 is on the scale of those at Site 724, roughly 2–3 m, and approximately half as thick as the cycles at Site 723 (Fig. 18).

Compressional-wave velocities measured with the *P*-wave logger are the only velocity data obtained at Site 727. Reliable *P*-wave logs were obtained to a depth of 38 mbsf in Hole 727A before sediment disturbance halted signal transmission through the core sections. Velocities range from 1520 to 1610 m/s and display a pattern of cyclic variation similar to that contained in the GRAPE records (Fig. 19).

Thermal Conductivity

Thermal conductivity measurements were made on alternate cores in Hole 727A through Core 117-727A-10X and on Cores 117-727B-1H and 117-727B-3H in Hole 727B (Table 7). The sediment conductivity ranges from 0.97 to 1.54 W·m^{-1}·K^{-1} and averages 1.23 W·m^{-1}·K^{-1}. With the exception of a low conductivity at 0.50 mbsf (0.95 W·m^{-1}·K^{-1}) and higher values between 12 and 18 mbsf (1.44–1.54 W·m^{-1}·K^{-1}) and 33 and 37 mbsf (1.34–1.37 W·m^{-1}·K^{-1}), most values are clustered about 1.2 W·m^{-1}·K^{-1} and there is little change in conductivity with depth (Fig. 20). Although the thermal conductivity of sediments

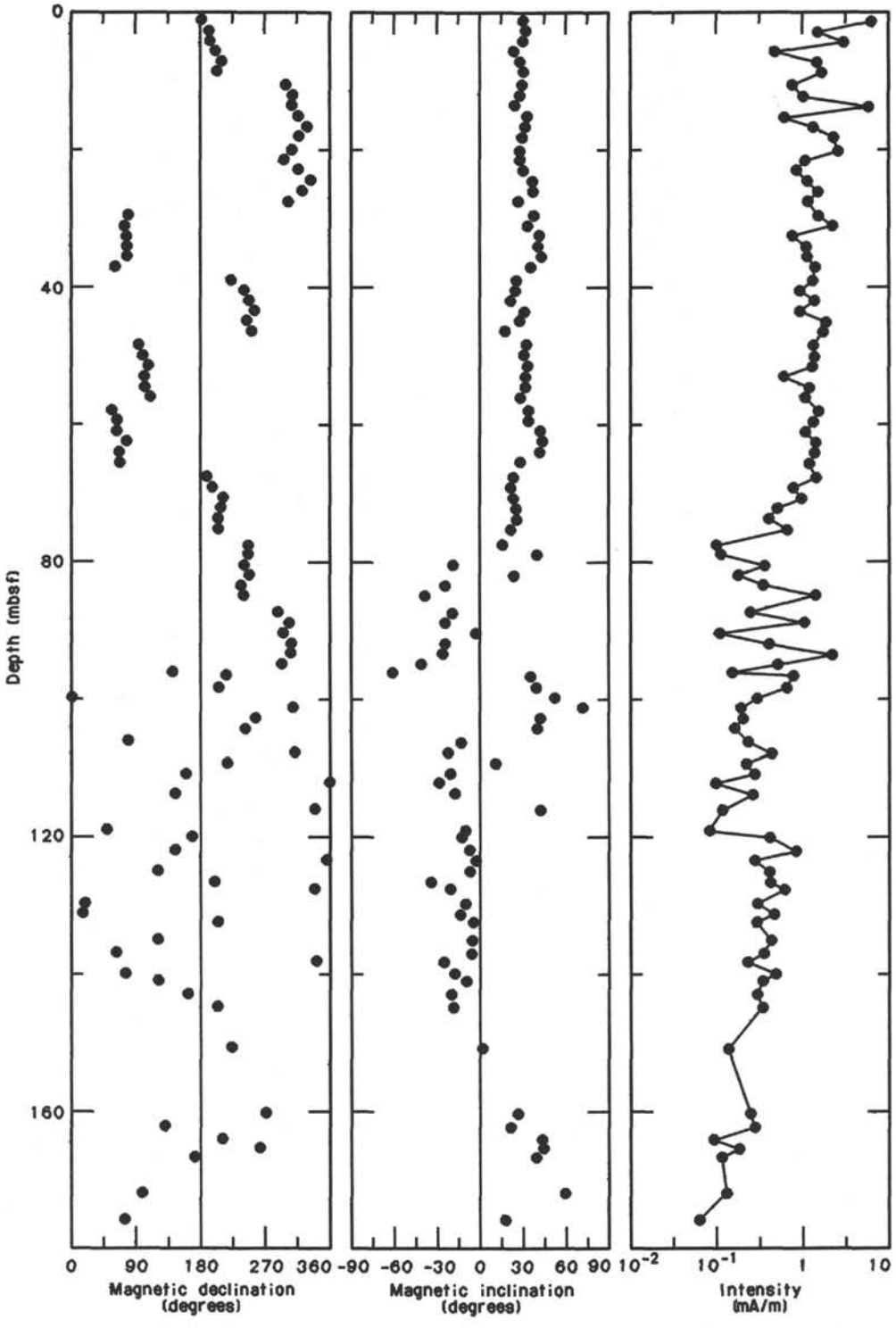

Figure 10. Plots of magnetic declination (relative values), inclination, and intensity against the sub-bottom depth of Hole 727A, obtained by shipboard measurements after AF demagnetization at 5 or 10 mT and filtering circular standard deviation values greater than 40°.

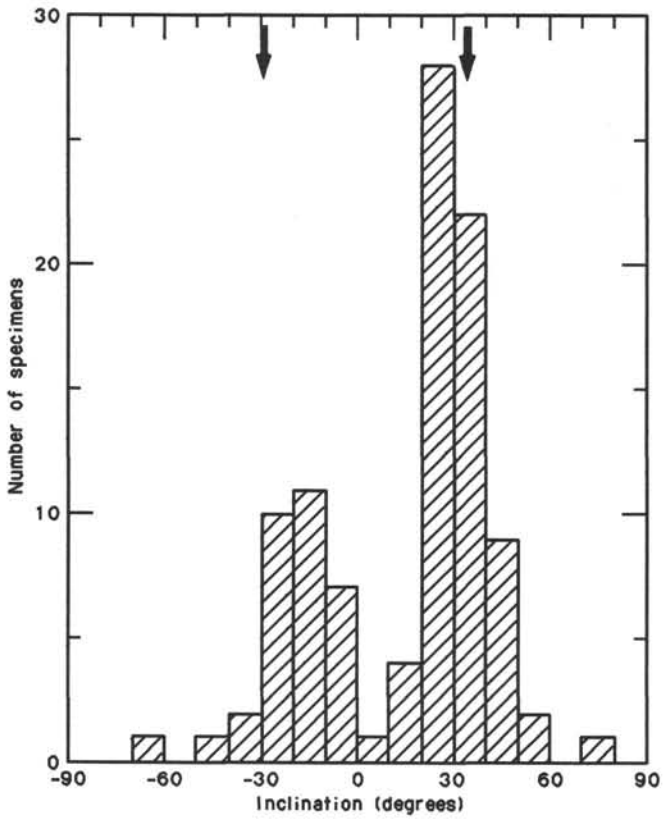

Figure 11. Histogram of magnetic inclination values from Site 727. Arrows show the values expected from the geocentric axial dipole field (32.7°).

Table 5. Magnetozone boundaries in Hole 727A.

Boundary	Age (Ma)	Core, section, interval (cm)	Depth (mbsf)
Brunhes/Matuyama (C1/C1r)	0.73 Ma	117-727A-9H-4, 115 to 117-727A-9H-5, 115	81.75–83.25
Top of Jaramillo (C1r/C1r-1)	0.91 Ma	117-727A-10H-8, 85 to 117-727A-11X-1, 101	95.87–96.41
Bottom of Jaramillo (C1r-1/C1r)	0.98 Ma	117-727A-11X-6, 124 to	104.14–106.01
Top of Olduvai (C1r/C2)	1.66 Ma	117-727A-17X-6, 107 to 117-727A-16X-5, 104	162.06–163.94

Note: Ages of chronozone boundaries are after Berggren et al., 1985b.

from Holes 727A and 727B does not appear to depend on burial depth over the measurement range, conductivity does display a strong positive correlation with wet-bulk density (Fig. 21).

Vane Shear Strength

Only three vane shear strength measurements were made on cores at Site 727 (Table 7). The shear strengths range from 16.2 kPa at 11.7 mbsf to 30.4 kPa at 21.1 mbsf.

INORGANIC GEOCHEMISTRY

Introduction

Nine interstitial water samples were collected at Site 727, seven by squeezing and two using the *in-situ* water sampling tool. All analytical data are listed in Table 8 and presented in Figure 22.

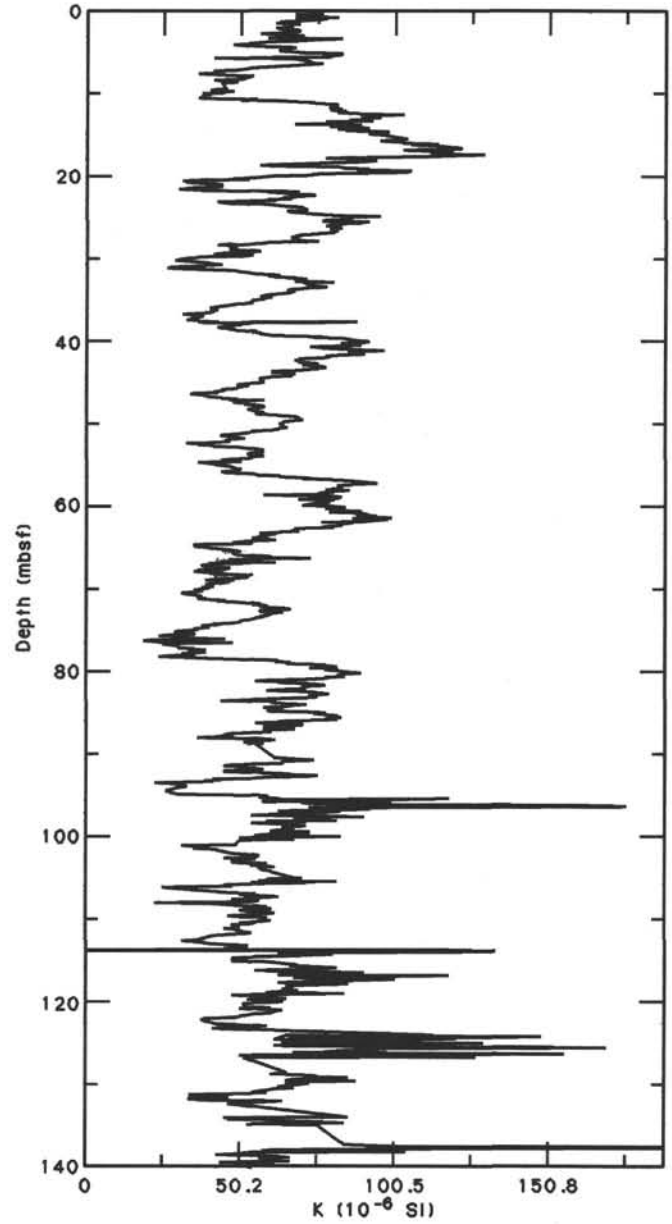

Figure 12. Plots of magnetic susceptibility data for Hole 727A.

Salinity, Chloride, and pH

Salinity decreases with depth, as we have observed at most other Oman margin sites (Fig. 22). This is attributable to the reduction of sulfate as well as a significant downward decrease in the magnesium content.

More important, the chloride concentration decreases from 569 mmol/L at the top of Hole 727A to 554 mmol/L at ~170 mbsf. A similar distribution was observed at Site 723, which we ascribed to the downward diffusion of chloride toward a more brackish fluid at depth, or the upward advection of such a fluid.

The pH appears to decrease with depth, but, as at other margin sites, the data are not considered to be reliable due to steady loss of CO_2 during pH measurement.

Sulfate and Alkalinity

The sulfate gradient over the upper 40 m at this site, ~ -0.5 mmol/L/m, is similar to that at Site 723. The sulfate concentra-

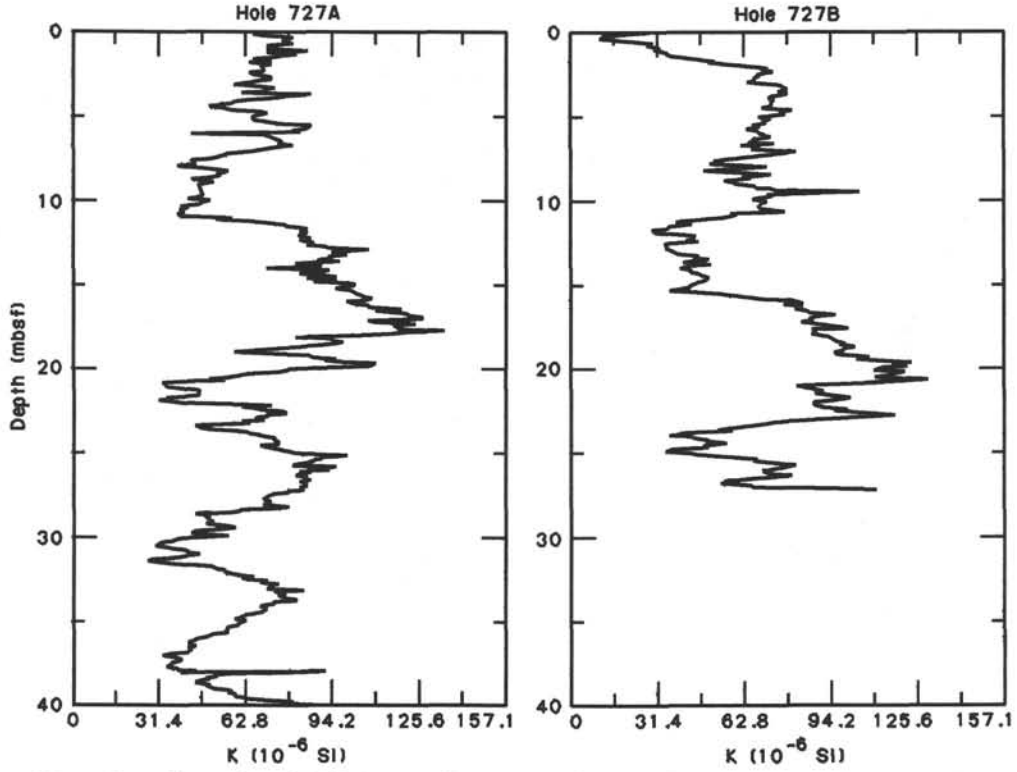

Figure 13. An illustration of the high-resolution stratigraphic utility of continuous magnetic susceptibility measurements. As shown by the susceptibility data of Hole 727B, the first core of Hole 727A missed the mud line and ~4 meters of surficial sediment.

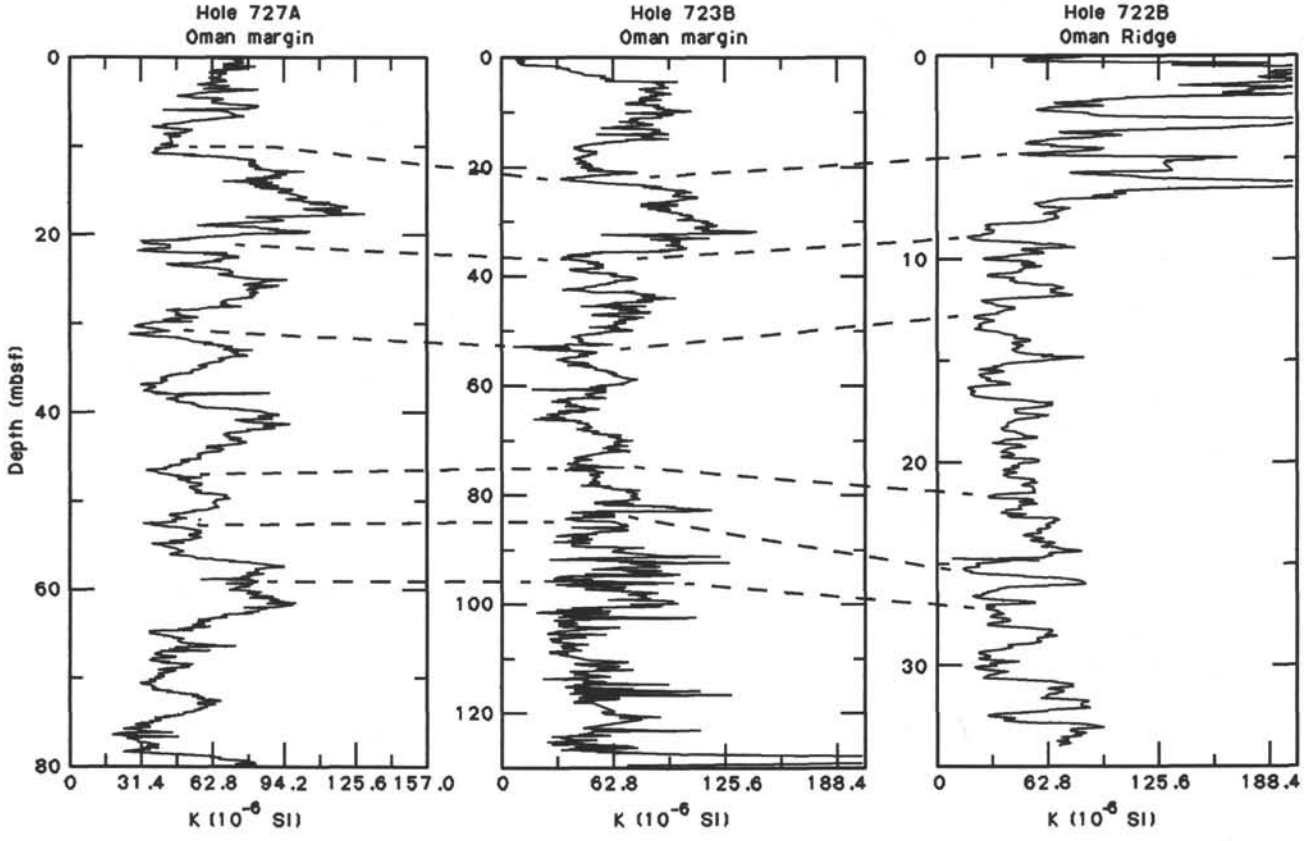

Figure 14. Brunhes Chronozone correlations between the magnetic susceptibility data of Holes 727A and 723B from the Oman margin and Hole 722B from the Owen Ridge.

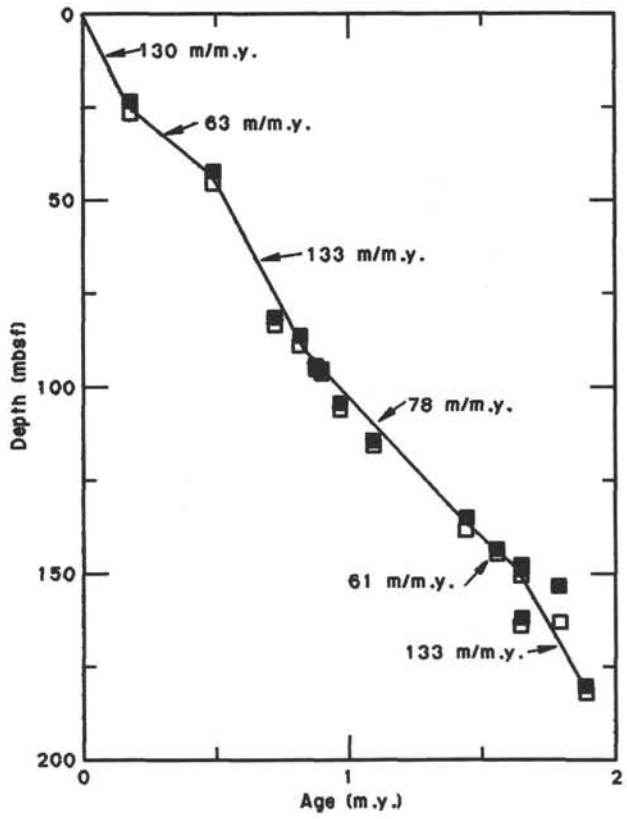

Figure 15. Age-depth plot of stratigraphic datums listed in Table 6. The filled and open dots are the upper and lower depths of each datum level, respectively. Indicated sedimentation rates (solid lines) are calculated between nannofossil datum levels whose ages are based on oxygen-isotope stratigraphy (N. Niitsuma, unpubl. data) or Berggren et al. (1985b).

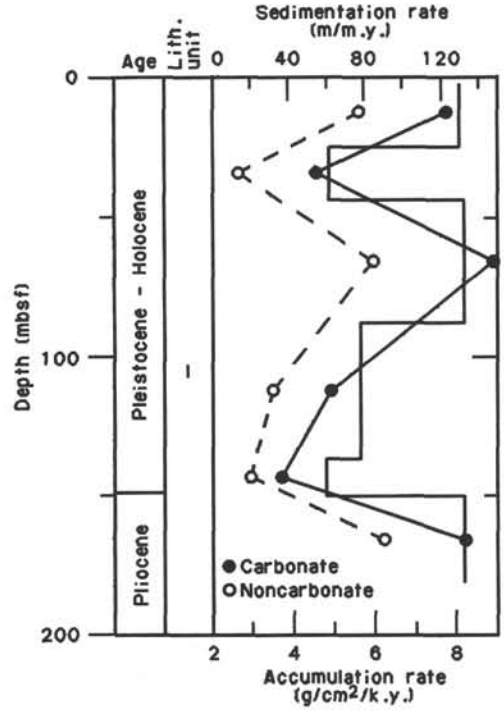

Figure 16. Sedimentation rate (m/m.y.; solid line), calcium carbonate accumulation rate (g/cm^2/k.y.; dots), and noncarbonate accumulation rate (g/cm^2/k.y.; circles) vs. depth at Site 727. Accumulation rates are plotted at the midpoint of the respective depth intervals.

tion falls to zero near 50 mbsf but increases at greater depths to levels >1 mmol/L (Table 8 and Fig. 22). As at Site 723, the presence of SO_4^{2-} in the lower half of the hole suggests that upward diffusion from a sulfate-enriched fluid at depth is responsible for the unusual distribution. Joint consideration of the sulfate and chloride profiles implies that the fluid may have been derived from the leaching of gypsum or anhydrite by relatively fresh water.

Moderate alkalinities are observed at Site 727. As we have discussed in previous reports for margin sites, the alkalinity distribution can be attributed to three processes: (1) production of HCO_3^- (which dominates), NH_4^+, and H_2S during sulfate reduction; (2) consumption of HCO_3^- by precipitating carbonate phases; and (3) production of NH_4^+ during methanogenesis. Process (1) appears to be restricted largely to the upper 50 m, although the reduction of upward-diffusing SO_4^{2-} at greater depths may be important. The calcium and magnesium profiles (see below) indicate that process (2) is important only in the top 50 m. The ~25 mmol/L increase in alkalinity between 50 and 180 mbsf corresponds to an increase of similar magnitude in the ammonia concentration (Fig. 22), suggesting that process (3) may be a major contributor to alkalinity below the upper zone of sulfate reduction.

Calcium and Magnesium

Most of the curvature in the calcium and magnesium profiles occurs in the top 60 m of the section (Fig. 22), suggesting that diagenetic reactions involving these ions are confined to this upper zone. The slight increase in the Mg^{2+}/Ca^{2+} ratio between 6 and 25 mbsf, coupled with a concurrent decrease in the calcium concentration, indicates that calcite may be precipitating in this interval. The decrease of magnesium between 25 and ~60 mbsf is attributed to the formation of dolomite in this zone. We cannot determine whether this occurs via replacement of pre-existing calcite or by direct precipitation. The flat nature of the profiles in the lower half of the section indicates that alteration of basement rocks is not influencing the distribution of dissolved magnesium and calcium over the top 200 m of the sedimentary column at this site.

Ammonia, Phosphate, Silica, and Dissolved Organic Carbon

A comparison of the ammonia and sulfate profiles indicates that ammonia must be being removed from solution over the top ~35 m of the cored section, presumably by the uptake of NH_4^+ by clay minerals (Fig. 22). The magnesium distribution does not indicate that ammonium is exchanging directly for magnesium in clays. The increase in the dissolved ammonia concentration below ~40 mbsf may reflect saturation of the clays by ammonia, although a generally higher organic carbon concentration in this zone could be related to enhanced ammonia production if the more abundant organic matter at depth had a lower C:N ratio (i.e., was less refractory).

Dissolved phosphate levels are much lower than would be predicted on the basis of the observed ammonia concentrations. As at other sites, the phosphate deficiency is probably due to the precipitation of apatite phases.

The rather low gradient of the dissolved silica profile (Fig. 22) over the top 40 m of the section (~20 μmol/L/m) indicates that the sediments at Site 727 are relatively depleted in opal. There is no indication in the profile that zones enriched in opal occur in the cored section.

The dissolved organic carbon (DOC) profile shown in Figure 23 and the data listed in Table 9 suggest that relatively high concentrations of sedimentary organic matter should be encountered at a depth of roughly 40 mbsf. However, the organic car-

Table 6. Sedimentation and accumulation rate data for Site 727.

Depth interval (mbsf)	Age range (m.y.)	$CaCO_3$ ($\bar{x}$ %)	C_{org} ($\bar{x}$ %)	Dry-bulk density ($\bar{x}$ g/cm^3)	Sed. rate ($\bar{x}$ m/m.y.)	$CaCO_3$ acc. rate (g/cm^2/k.y.)	Non-$CaCO_3$ acc. rate (g/cm^2/k.y.)	C_{org} acc. rate (mg/cm^2/k.y.)
0–24.6	0–0.19	58.0	2.57	1.03	129.5	7.74	5.60	342.8
24.6–43.5	0.19–0.49	63.2	0.80	1.14	63.0	4.54	2.64	57.5
43.5–87.3	0.49–0.82	59.9	1.42	1.12	132.7	8.90	5.96	211.0
87.3–136.5	0.82–1.45	58.4	2.79	1.08	78.1	4.93	3.51	235.3
136.5–149.3	1.45–1.66	55.9	4.51	1.10	61.0	3.75	2.96	302.6
149.3–181.2	1.66–1.90	56.8	2.75	1.09	132.9	8.23	6.26	398.4

bon distribution reported in the "Organic Geochemistry" section (this chapter) indicates that DOC and sedimentary organic carbon distributions are poorly correlated at this site. We do not know why the correlation is excellent at some sites (e.g., Site 728) and not at others. The differences may be related to spatial and/or temporal variations of either the type or quality (i.e., extent of degradation) of buried organic matter.

ORGANIC GEOCHEMISTRY

Organic Matter Abundance and Character

We investigated 30 sediment samples from Hole 727A by carbon analysis and Rock-Eval pyrolysis. Organic carbon concentrations average 2.51% and range from 0.80% to 4.96% in the only lithologic unit recognized (Table 3 and Fig. 24).

A slight trend to high organic carbon values as well as high hydrogen index values appears with depth in Figure 24. Assuming a uniform sedimentation rate, the variation in organic carbon concentrations might be the sedimentary expression of variations in the primary productivity.

When the hydrogen and oxygen indices of samples from Site 727 (Table 10) are plotted in a "van Krevelen-type" diagram together with these indices from Site 722 on the Owen Ridge (dots) and from Site 726 on the Oman margin (triangles), samples from Hole 727A (diamonds) plot for the most part in a cluster characterized by a hydrogen index between 200 and 400, and an oxygen index less than 150 (Fig. 25). This may be viewed as a manifestation of the relatively pristine nature of organic matter deposited under oxygen-depleted conditions at the center of the OMZ at Site 727, as compared with organic matter buried under oxygenated water at Site 722 (2034-m water depth). The wide spread of values from Site 726 may be due to sporadically oxic/suboxic/anoxic conditions prevalent at Site 726 (water depth 331 m). Alternatively, the source of the organic matter may be different in the three sectors of the upwelling system and may be related to a spatial zonation of primary producers.

Hydrocarbon Gases

The rapid decrease of interstitial sulfate to negligible amounts below 60 mbsf (see "Inorganic Geochemistry" section, this chapter) is mirrored by a steady increase of biogenic methane measured in headspace samples (Fig. 26 and Table 11). Below the depth of sulfate depletion, we observed the first gas pockets, almost entirely composed out of biogenic methane with small amounts of thermogenic ethane and propane in the hydrocarbon fraction (Table 12). The increase of ethane and propane concentration with depth (Figs. 26 and 27) is in concordance with findings at other sites on the Oman margin.

INTERHOLE CORRELATION

The two holes drilled at Site 727 are located at 915 mbsl in the southern part of the slope basin, previously drilled at Site 723. Holes 727A and 727B were drilled without offset; Hole 727A was drilled to 95.4 mbsf with the APC and to 182.4 mbsf with the XCB, while Hole 727B penetrated 27.1 mbsf with the APC. Recovery from APC coring was almost perfect in these holes, and the top of Hole 727B obtained the mud line.

Detailed correlations in the upper 55 m of the drilled sediments at Site 727 are given here. The upper interval has an age range from 0 to about 0.5 Ma, and is characterized by cyclic changes in the nature of sediments that can be identified by visual observation and by variations of magnetic susceptibility and $CaCO_3$ content. The coherence and similarity of sediments among these holes provides valuable information on the relative rate of sedimentation, which is necessary information for any high-resolution study of depositional environments. The essence of the interhole correlation process is outlined in the "Explanatory Notes" chapter.

Hole-to-hole correlations were made on the basis of visual identification of distinctive layers, as well as physical and magnetic properties. Magnetic susceptibility was measured at 10-cm intervals before splitting the sections. Photographs were taken of the split cores.

Visual correlation of the cores relied primarily on the core photographs. We determined 26 distinct and traceable layers in the upper 55 m of sediment at Sites 723 and 724, which have been denoted as OM-a_1, ..., h_3, and h_5, based on the correlation between the holes at Sites 723 and 724 (see "Interhole Correlation" sections, "Site 723" and "Site 724" chapters). The letter code (i.e., a, b, c, ...) refers to the sequence of cores, and the number subscript indicates the marker layer sequence in each core. For example, the notation "a_2" corresponds to the second marker layer defined in Core 117-723A-1H, and "b_1" denotes the first marker layer in Core 117-723A-2H. The marker layers a_1–h_4 were defined on the cored sediments of Hole 723A. Three marker layers (c_5, e_3, and h_5) were defined on the sedimentary sequence at Hole 724A in addition to those noted at Site 723.

The criteria for defining a marker layer are that the layer is distinct enough to trace in the sedimentary sequence of the other holes and that its character does not change. The useful criteria for recognizing the marker are color boundaries, distinctly colored layers, shape of bioturbation, and sequence of color change in surrounding sediments. Table 13 lists the depth of the marker layers in two holes of Site 727.

Figure 28 shows the magnetic susceptibility curve and positions of individual, visually correlatable layers. The pattern of the susceptibility and the positions of layers match very well, not only among the two holes, but also between Sites 723 and 727 (Fig. 28). The stratigraphy of the magnetic susceptibility data and the visually identified layers are extremely consistent in that a particular visually characteristic layer always coincides in depth with a distinct feature in the magnetic susceptibility curve. In this way the lithologic marker layer correlations are confirmed using the susceptibility data, which are quantitative.

The results of the layer-by-layer correlation allow us to calculate the true thickness of these layers that coincide with and are separated by core boundaries. Core tops occasionally were ex-

Table 7. Physical properties summary, Hole 727A.

Core, section, interval (cm)	Depth (mbsf)	Wet-bulk density (g/cm^3)	Porosity (%)	Water content (%)	Grain density (g/cm^3)	Dry-bulk density (g/cm^3)	Thermal conductivity ($W \cdot m^{-1} \cdot K^{-1}$)	Vane shear strength (kPa)
117-727A-								
1H-2, 100–102	2.50	1.589	65.7	42.4	2.614	0.915		
1H-4, 100–102	5.50	1.650	54.3	33.7	2.599	1.094		
1H-6, 100–102	8.50	1.572	67.0	43.7	2.564	0.885		
2H-2, 50–52	11.50	1.761	55.4	32.2	2.599	1.193		
2H-2, 100–101	12.00						1.44	
2H-4, 50–52	14.50	1.759	58.4	34.0	2.700	1.161		
2H-4, 100–101	15.00						1.54	
2H-6, 50–52	17.50	1.734	56.4	33.3	2.560	1.156		29.0
2H-6, 100–101	18.00						1.13	
3H-2, 100–102	21.40	1.551	67.0	44.2	2.548	0.865		
3H-4, 78–80	24.18	1.582	57.3	37.1	2.583	0.995		
3H-6, 36–38	26.76	1.814	61.5	34.7	2.689	1.184		
4H-2, 6–8	29.96	1.624	64.0	40.4	2.589	0.968		
4H-2, 80–81	30.70						1.20	
4H-4, 6–8	32.96	1.803	53.4	30.3	2.534	1.256		
4H-4, 80–81	33.70						1.37	
4H-6, 6–8	35.96	1.691	61.0	36.9	2.650	1.066		
4H-6, 80–81	36.70						1.34	
5H-2, 71–73	40.01	1.848	51.3	28.4	2.642	1.323		
5H-4, 32–34	42.62	1.677	59.4	36.3	2.501	1.068		
6H-2, 50–52	49.30	1.691	56.6	34.3	2.535	1.112		
6H-2, 80–81	49.60						1.27	
6H-4, 80–81	52.60						1.15	
6H-4, 111–113	52.91	1.699	61.6	37.1	2.678	1.068		
6H-6, 8–10	54.88	1.608	62.5	39.8	2.469	0.968		
6H-6, 80–81	55.60						1.17	
7H-2, 123–125	59.53	1.753	56.5	33.0	2.592	1.175		
7H-4, 8–10	61.38	1.786	53.5	30.7	2.563	1.238		
7H-6, 8–10	64.38	1.639	65.0	40.6	2.633	0.973		
8H-2, 24–26	68.14	1.680	61.8	37.7	2.643	1.047		
8H-2, 78–79	68.68						1.20	
8H-4, 40–42	71.30	1.628	61.1	38.4	2.445	1.002		
8H-4, 78–79	71.68						1.20	
8H-6, 8–10	73.98	1.748	58.6	34.4	2.677	1.147		
8H-6, 78–79	74.68						1.16	
9H-3, 27–29	79.37	1.848	50.8	28.2	2.639	1.328		
9H-6, 63–65	84.23	1.797	55.8	31.8	2.662	1.226		
10X-2, 75–76	86.77						1.16	
10X-3, 80–82	88.32	1.670	62.0	38.0	2.590	1.035		
10X-4, 75–76	89.77						1.24	
10X-5, 90–92	91.42	1.717	60.7	36.2	2.694	1.095		
10X-6, 75–76	92.77						1.21	
10X-7, 88–90	94.40	1.697	59.8	36.1	2.570	1.084		
11X-2, 76–78	97.66	1.720	59.0	35.1	2.601	1.116		
11X-4, 25–27	100.15	1.656	61.0	37.7	2.559	1.031		
11X-6, 85–87	103.75	1.755	57.3	33.5	2.629	1.168		
12X-2, 98–100	107.48	1.723	60.4	35.9	2.660	1.104		
12X-4, 98–100	110.48	1.749	56.3	33.0	2.615	1.172		
12X-6, 98–100	113.48	1.712	58.7	35.1	2.562	1.111		
13X-2, 93–95	117.03	1.765	58.0	33.6	2.667	1.171		
13X-4, 102–104	120.12	1.706	60.1	36.1	2.594	1.090		
13X-6, 80–82	122.90	1.671	60.0	36.8	2.515	1.057		
14X-2, 98–100	126.48	1.638	63.2	39.5	2.557	0.990		
14X-4, 133–135	129.83	1.687	59.1	35.9	2.561	1.082		
14X-7, 18–20	133.18	1.654	61.5	38.1	2.536	1.023		
15X-2, 28–30	135.68	1.660	61.6	38.0	2.597	1.028		
15X-4, 17–19	138.57	1.638	60.6	37.9	2.464	1.017		
15X-6, 58–60	141.98	1.685	57.9	35.2	2.433	1.092		
16X-2, 80–82	145.90	1.655	58.4	36.1	2.434	1.058		
16X-4, 60–62	148.70	1.812	54.6	30.9	2.641	1.252		
16X-6, 114–116	152.24	1.701	57.8	34.8	2.518	1.109		
17X-2, 94–96	155.74	1.754	58.8	34.4	2.668	1.151		
17X-4, 95–97	158.75	1.691	59.8	36.2	2.556	1.079		
17X-6, 120–122	162.00	1.700	57.7	34.8	2.521	1.109		
18X-2, 84–86	165.34	1.690	60.4	36.6	2.610	1.071		
18X-4, 104–106	168.54	1.643	62.5	38.9	2.572	1.003		
18X-6, 98–100	171.48	1.663	61.7	38.0	2.568	1.031		
19X-1, 135–137	174.05	1.692	58.8	35.6	2.525	1.090		
19X-3, 128–130	176.98	1.731	60.6	35.8	2.639	1.111		
19X-5, 95–97	179.65	1.751	56.0	32.8	2.576	1.178		
117-727B-								
1H-1, 50–51	0.50					0.970		
1H-3, 50–52	3.50	1.569	66.4	43.3	2.510	0.889	1.19	
1H-5, 50–51	6.50						1.23	
2H-3, 50–52	11.70	1.465	72.8	50.9	2.544	0.719		16.2
3H-1, 50–51	18.10						1.44	
3H-3, 50–52	21.10	1.529	67.3	45.1	2.438	0.839	1.14	30.4
3H-5, 50–51	24.10						1.17	

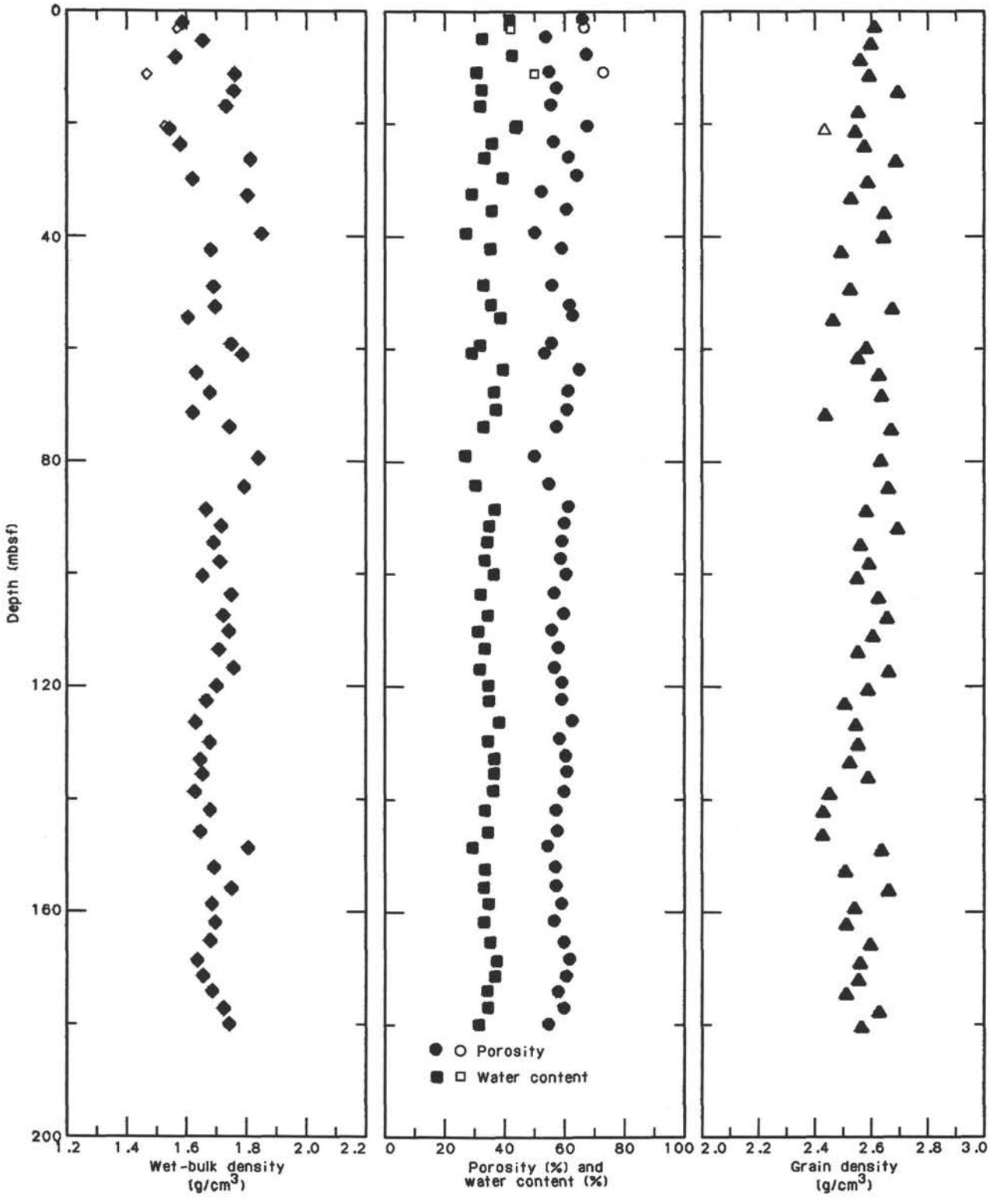

Figure 17. Index properties (wet-bulk density, porosity, water content, and grain density) measured on discrete samples from Holes 727A and 727B. Closed symbols represent values for Hole 727A, and open symbols, Hole 727B.

panded by water uptake during drilling. In this case, the apparent thickness of the disturbed sediment layer is observed to be thicker than the original thickness. In some instances, the top part of the core was missing; in this case, apparent thickness is observed to be thinner than the original thickness. Fortunately, the two holes were staggered in depth so that they have different horizons at core boundaries (Table 13).

The original thickness of layers coinciding with core tops or bottoms can be obtained by comparing the thickness of the correlative layer in the continuous section of the other holes. The

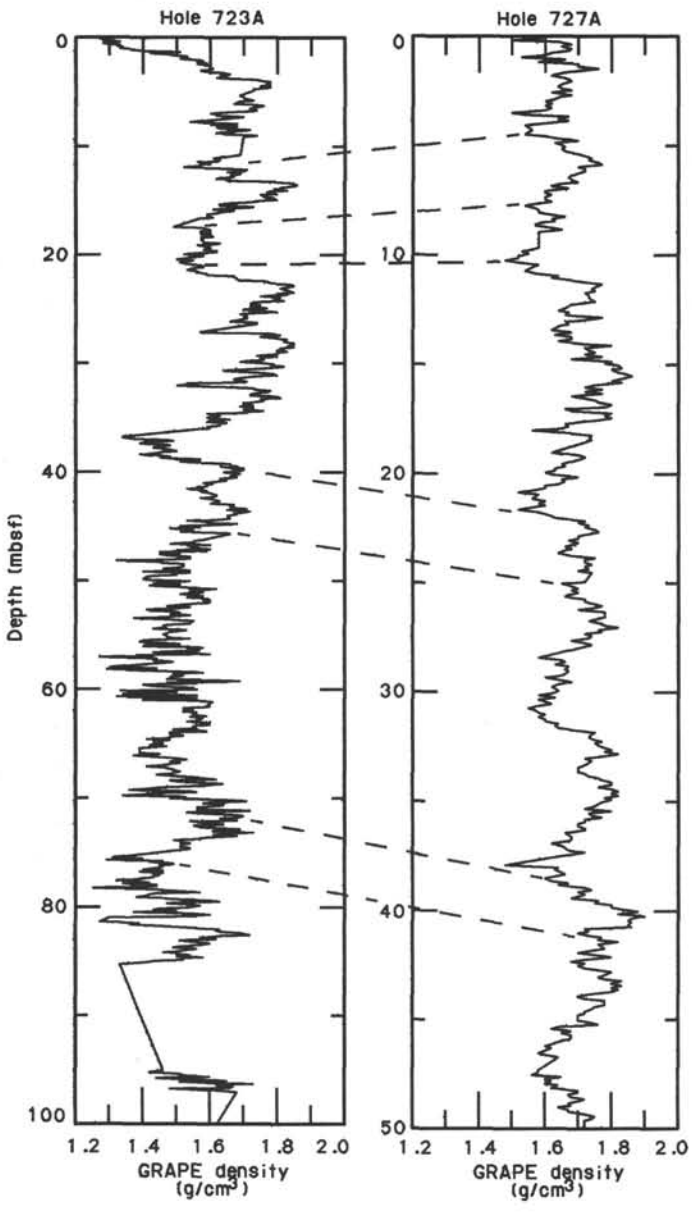

Figure 18. GRAPE wet-bulk density for Holes 723A and 727A. The profiles are based on 10-cm-block averages of the data. Note that the depth scale for Hole 723A is approximately half that of Hole 727A.

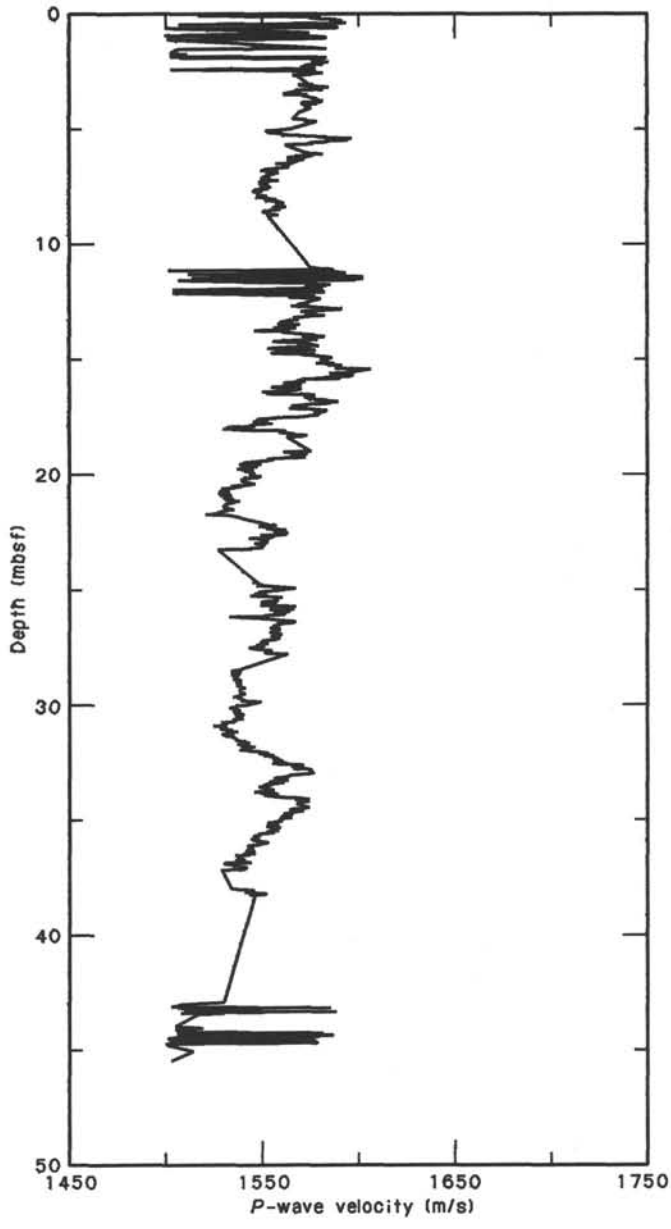

Figure 19. Compressional-wave velocity as measured by the *P*-wave logger in Hole 727A.

calculation of the amount of the difference can be achieved by the differences in the ODP depths of marker layers between the holes ("727B – 727A" in Table 13). Table 14 gives the differences between the depth (mbsf) calculated by the ODP CORELOG data and the corrected depth (mbsf) calculated by the layer-by-layer correlation method.

The layer-by-layer method on the double-cored sedimentary sequences gives us true stratigraphic thickness after the correction for core-boundary disturbance. Table 15 shows the stratigraphic thickness at Sites 723 and 724, where the marker layers were defined, and Holes 727A and 727B. The corrected depths in Hole 727A and 727B agree well with each other. The intersite correlation of the marker layers shows clearly the differences in the rate of sedimentation.

SUMMARY AND CONCLUSIONS

Site 727 is located in the northwestern Arabian Sea on the Oman continental margin and corresponds to a second drilling target (in addition to Site 723) near the center of a slope basin. The water depth of Site 727 (914 m) lies near the bottom of the pronounced OMZ that impinges on the continental margin underneath a zone of high biogenic productivity. Site 727 was located in the southern part of a slope basin formed by a narrow half-graben in what is presumed to be ophiolitic basement. Biogenic material produced by coastal upwelling and eolian components are deposited here at high rates (~95 m/m.y.). Our intentions in drilling Site 727 were (1) to complement the continuous and expanded sections of upper Neogene to Recent sediments previously recovered at Site 723, (2) to trace the imprint of the OMZ through time, and (3) to investigate diagenetic sedimentary processes.

Some of the major findings at Site 727 are summarized in Figure 29 and include the identification of

1. a uniform lithology, lacking laminations and silica, ranging in age from latest Pliocene to Holocene;

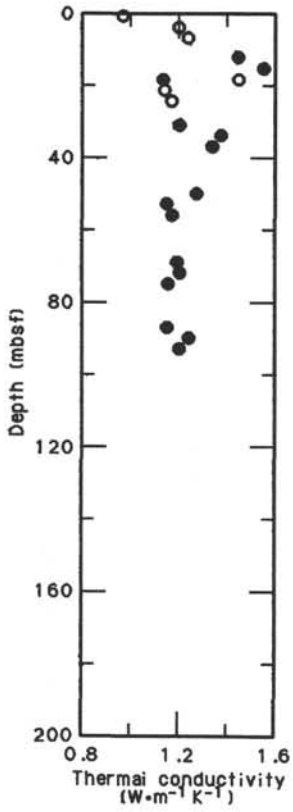

Figure 20. Thermal conductivity vs. depth for Holes 727A (dots) and 727B (circles).

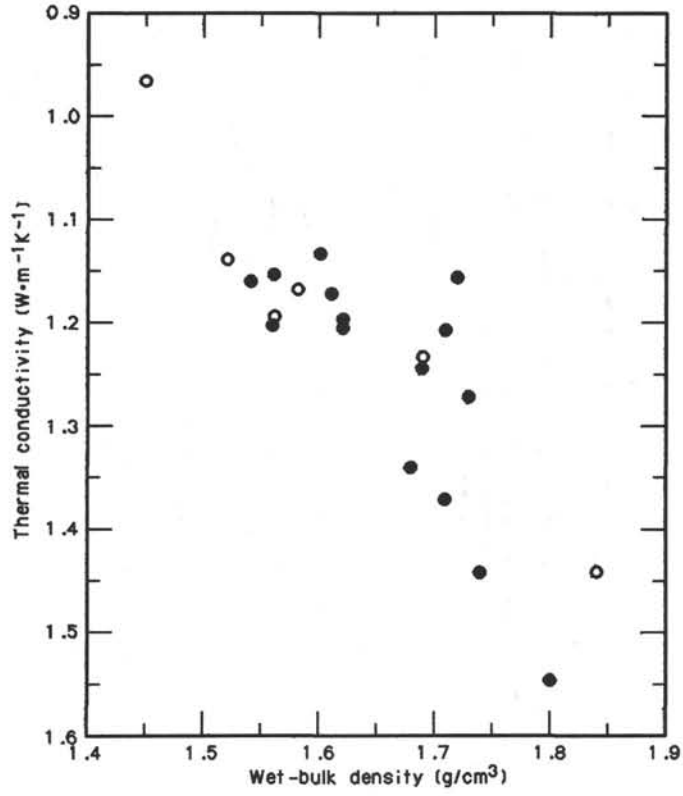

Figure 21. Thermal conductivity vs. wet-bulk density for Holes 727A (dots) and 727B (circles). GRAPE data were used to estimate wet-bulk density for intervals of conductivity measurement which lack a corresponding discrete-sample wet-bulk density determination.

2. calcareous nannofossils that are indicative of cold water and upwelling and that occur in the lower Pleistocene (traces of opal are found only in the uppermost Pliocene); and

3. complete sulfate depletion by 50 mbsf but increasing sulfate downsection associated with a continuous downsection increase in alkalinity.

The section penetrated at Site 727 ranges from uppermost Pliocene to Holocene. The magnetostratigraphy at Site 727 was especially well defined so that the Brunhes-Matuyama boundary, the Jaramillo subchronozone, and the top of the Olduvai were identified.

Only one lithologic unit was recognized at Site 727. The unit comprises homogeneous green to olive green foraminifer-bearing marly nannofossil ooze and calcitic marly nannofossil ooze. The calcium carbonate and organic carbon contents of this facies vary between 40% to 70% and 1% to 7%, respectively. The mean sedimentation rates at Site 727 (60–133 m/m.y.) are consistently lower than those at Site 723 (129–240 m/m.y.), and the section appears to have been deposited continuously. Magnetic susceptibility shows consistent downhole variability that correlates with other margin and ridge sites and reflects climate-related changes in the depositional system, which is dominated by upwelling and eolian input.

The benthic foraminifers are more abundant at Site 727 than at any of the margin sites, but they show few faunal changes, indicating little or no changes due to increasing depth. Faunal and floral assemblages indicate that monsoonal upwelling was persistent throughout the time of deposition. However, some calcareous nannoplankton indicator species only occur in the upper Pliocene and lower Pleistocene. Opal occurs only in traces during this same interval.

Chemical compositions of interstitial waters show a downsection increase, indicating a possible sub-bottom supply of sulfate. Diagenetic remineralization at Site 727 appears to be dominated by fermentation reactions and methanogenesis. Similar to previous sites on the margin, Site 727 showed a strong increase in ethane and propane with depth.

Site 727 provides confirmation of many of the biotic and depositional trends observed at other sites on the Oman margin. However, the lack of laminated facies at Site 727, which lies at the same depth and covers the same time span as Site 723, poses questions about the heterogeneity of the processes, such as the OMZ, that preserve the laminated facies.

REFERENCES

Berggren, W. A., Kent, D. V., Flynn, J. J., and Van Couvering, J. A., 1985a. Cenozoic geochronology. *Geol. Soc. Am. Bull.*, 96:1407–1418.

Berggren, W. A., Kent, D. V., and Van Couvering, J. A., 1985b. The Neogene: Part 2, Neogene geochronology and chronostratigraphy. *In* Snelling, N. J. (Ed.), *The Chronology of the Geological Record*, Geol. Soc. Mem. (London), 10:211–260.

Sato, T., Takayama, T., Kato, M., Kudo, T., and Kameo, K., in press. Calcareous microfossil biostratigraphy of the uppermost Cenozoic formations distributed in the coast of the Japan Sea. Part 4: Conclusion. *Sekiyu Gijutsu Kyokaishi.*

Takayama, T., and Sato, T., 1987. Coccolith biostratigraphy of the North Atlantic Ocean, Deep Sea Drilling Project Leg 94. *In* Ruddiman, W. F., Kidd, R. B., Thomas, E., et al., *Init. Repts. DSDP*, 94, Pt. 2: Washington (U.S. Govt. Printing Office), 651–702.

Ms 117A-114

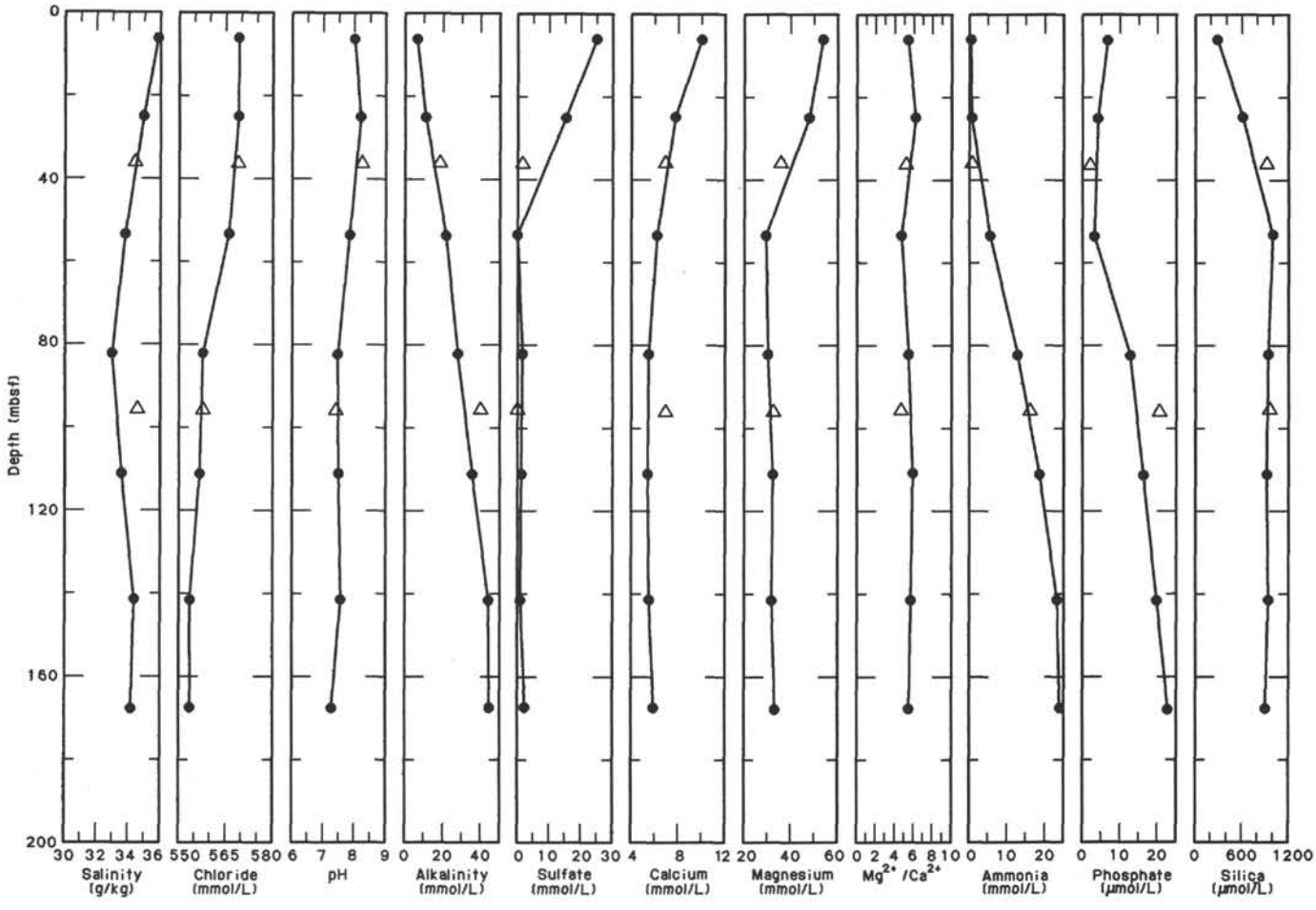

Figure 22. Concentration profiles vs. depth for Site 727.

Table 8. Summary of interstitial water geochemical data, Site 727.

Core, section, interval (cm)	Depth (mbsf)	Vol. (ml)	pH	Alk. (mmol/L)	Sal. (g/kg)	Mg (mmol/L)	Ca (mmol/L)	Cl (mmol/L)	SO_4 (mmol/L)	PO_4 (µmol/L)	NH_4 (mmol/L)	SiO_2 (µmol/L)	Mg/CA
1H-4, 145–150	5.95	47	7.99	6.34	35.8	53.49	9.94	569	24.6	5.5	0.50	285	5.38
3H-4, 145–150	24.85	54	8.19	10.96	34.9	47.81	7.75	569	15.2	3.0	0.64	603	6.17
4I-6, 0–1	35.90	10	8.26	18.26	34.4	36.09	6.91	569	1.6	1.1	0.82	925	5.22
6H-4, 145–150	53.25	47	7.86	21.48	33.8	29.89	6.27	566	0	2.3	5.59	990	4.77
9H-4, 145–150	82.05	36	7.48	27.60	33.0	30.76	5.56	558	1.6	11.6	12.71	940	5.53
11I-1, 0–1	95.40	10	7.42	39.57	34.6	32.94	6.96	558	0	19.1	16.08	953	4.73
12X-4, 145–150	110.95	37	7.51	35.34	33.6	32.68	5.47	557	1.3	15.0	18.57	923	5.97
15X-5, 145–150	141.35	36	7.58	44.07	34.4	32.33	5.58	554	1.0	18.6	23.29	942	5.79
18X-3, 145–150	167.45	50	7.30	44.56	34.2	33.66	6.00	554	2.4	21.6	24.08	904	5.61

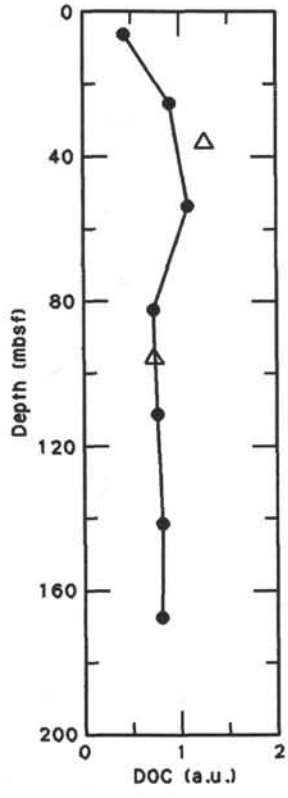

Figure 23. Dissolved organic carbon (DOC) profile for Site 727 in absorbance units (a.u.). Triangles represent the *in-situ* samples.

Table 9. Relative dissolved organic carbon concentrations at Site 727.

Core, section, interval (cm)	Dissolved organic carbon (a.u.)
117-727A-	
1H-4, 145–150	0.437
3H-4, 145–150	0.894
41-4, 0–1	1.260
6H-4, 145–150	1.087
9H-4, 145–150	0.730
11I-1, 0–1	0.743
12X-4, 145–150	0.769
15X-5, 145–150	0.820
18X-3, 145–150	0.805

Note: a.u. = absorbance units.

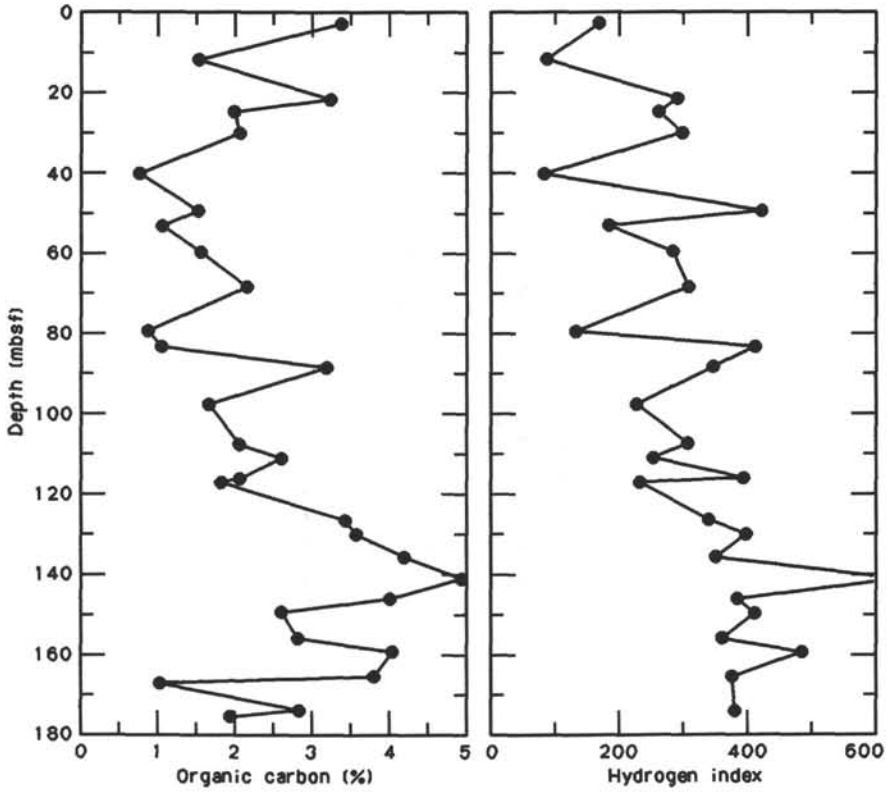

Figure 24. Downhole plot of organic carbon and the hydrogen index values from Rock-Eval pyrolysis.

Table 10. Results of Rock-Eval pyrolysis of samples from Hole 727A.

Core, section, interval (cm)	Depth (mbsf)	T_{max} (°C)	S_1	S_2	S_3	S_2/S_3	TOC	HI	OI
1H-2, 100–102	2.50	418	1.07	5.82	2.97	1.95	3.41	170	87
2H-2, 50–52	11.50	419	0.26	1.40	1.55	0.90	1.55	90	100
3H-2, 100–102	21.40	415	1.77	9.63	3.35	2.87	3.28	293	102
3H-4, 119–120	24.59	415	0.88	5.32	2.44	2.18	2.02	263	120
4H-2, 6–8	29.96	416	0.97	6.34	2.66	2.38	2.11	300	126
5H-2, 71–73	40.01	417	0.08	0.71	1.24	0.57	0.80	88	155
6H-2, 50–52	49.30	417	0.90	6.66	2.51	2.65	1.57	424	159
6H-4, 119–120	52.99	417	0.37	2.07	2.00	1.03	1.09	189	183
7H-2, 123–125	59.53	413	0.56	4.59	2.24	2.04	1.60	286	140
8H-2, 24–26	68.14	418	0.94	6.93	2.43	2.85	2.22	312	109
9H-3, 27–29	79.37	416	0.23	1.27	1.38	0.92	0.92	138	150
9H-5, 119–120	83.29	411	0.80	4.57	1.85	2.47	1.10	415	168
10H-3, 80–82	88.32	414	1.69	11.38	3.34	3.40	3.25	350	102
11H-2, 76–78	97.66	413	0.50	3.91	2.28	1.71	1.70	230	134
12H-2, 98–100	107.48	433	0.80	6.65	2.78	2.39	2.14	310	129
12H-4, 144–145	110.94	415	1.03	6.86	2.34	2.93	2.66	257	87
13H-2, 0–1	116.10	414	1.18	8.39	2.69	3.11	2.12	395	126
13H-2, 93–95	117.03	418	0.59	4.43	2.37	1.86	1.87	237	127
14H-2, 98–100	126.48	411	2.01	11.89	3.64	3.26	3.47	342	104
14H-4, 149–150	129.99	406	3.42	14.58	3.53	4.13	3.64	400	96
15H-2, 28–30	135.68	415	2.08	15.05	4.27	3.52	4.23	355	100
15H-5, 119–120	141.09	402	6.01	31.50	4.57	6.89	4.96	635	92
16H-2, 80–82	145.90	406	3.20	15.71	4.10	3.83	4.06	386	100
16H-4, 149–150	149.59	408	1.90	10.98	2.65	4.14	2.65	414	100
17H-2, 94–96	155.74	408	1.98	10.38	3.76	2.76	2.87	361	131
17H-5, 0–1	159.30	407	4.18	19.81	3.63	5.45	4.07	486	89
18H-2, 84–86	165.34	413	2.32	14.38	4.00	3.59	3.82	376	104
19H-1, 135–137	174.05	415	1.67	10.85	3.42	3.17	2.85	380	120

Note: HI = hydrogen index and OI = organic index. For a detailed description of parameters, see "Explanatory Notes" chapter (this volume).

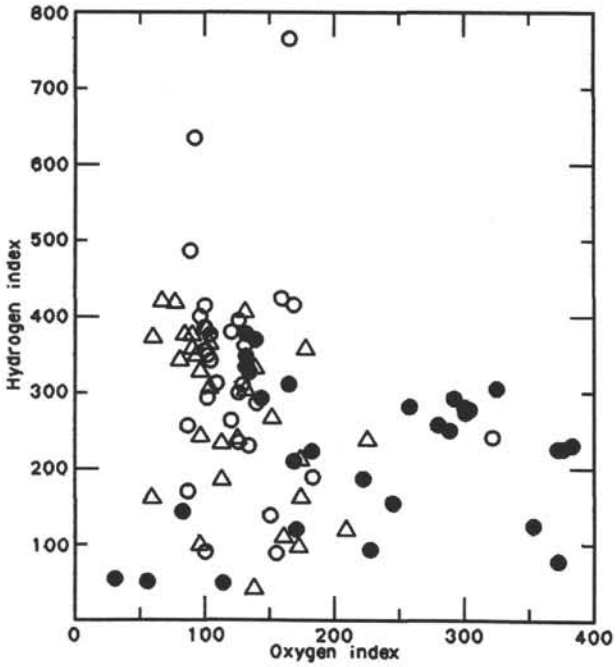

Figure 25. Plot of hydrogen vs. oxygen index of samples from Hole 727A (diamonds), Site 722 (dots), and Site 726 (triangles).

Table 11. Results of headspace analysis of interstitial gas at Hole 727A.

Core, section, interval (cm)	Depth (mbsf)	C_1 (mL/L)	C_2 (μL/L)	C_3 (μL/L)
3H-4, 119–120	24.59	77	2	
9H-5, 119–120	83.29	80813	10	3
12X-4, 144–145	110.94	66321	9	
13X-2, 0–1	116.10	103211	17	4
14X-4, 149–150	129.99	70643	26	10
15X-5, 119–120	141.09	57481	60	26
16X-4, 149–150	149.59	65125	30	10
17X-5, 0–1	159.30	77434	58	22
18X-3, 119–120	167.19	87741	30	13
19X-3, 0–1	175.70	107735	45	20

Note: Values are expressed as μL/L (volume gas/volume wet sediment).

Table 12. Results of gas analysis of vacutainer samples from Hole 727A.

Core, section, interval (cm)	Depth (mbsf)	C_1 (ppm)	C_2 (ppm)	C_3 (ppm)	C_1/C_2
8H-2, 40	68.30	1024211	70	3	14631
9H-6, 140	85.00	972155	74	4	13137
10H-6, 75	92.77	1027567	79	4	13007
11X-6, 27	103.17	1015621	83	4	12236
12X-5, 50	111.50	863423	73	4	11828
13X-6, 70	122.80	945271	93	5	10164
14X-5, 105	131.05	932922	111	6	8405
15X-4, 140	139.80	950363	101	5	9410
16X-5, 145	151.05	1002150	105	6	9544
17X-5, 75	160.05	984137	121	7	8133
18X-5, 105	170.05	946265	139	10	6808

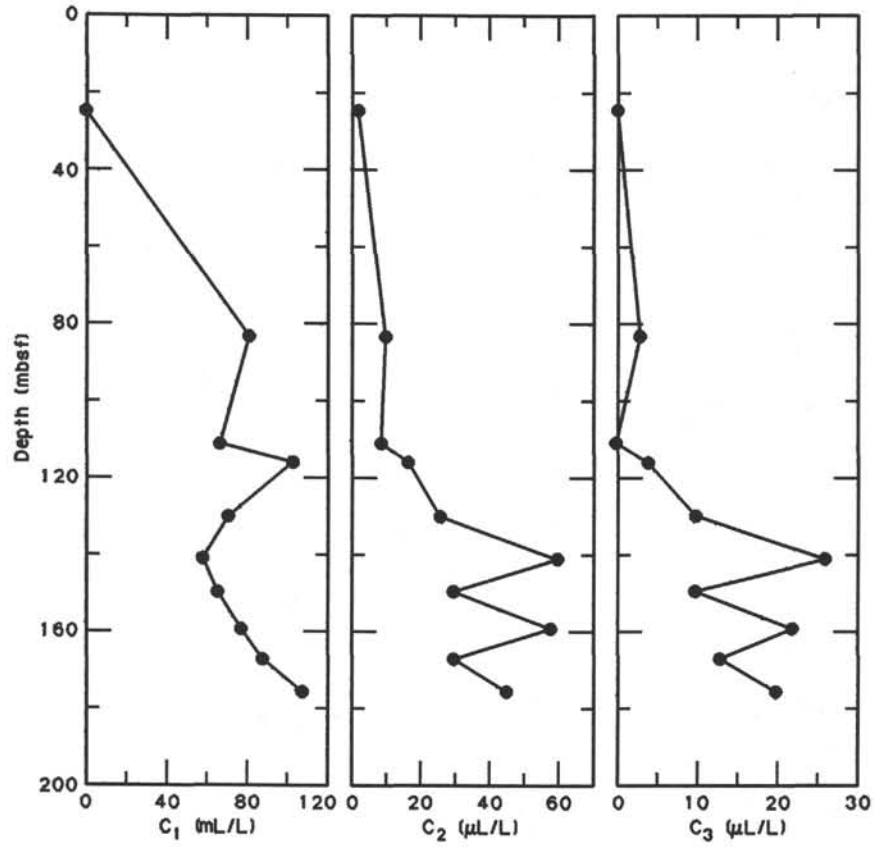

Figure 26. Downhole plot of methane (C_1), ethane (C_2), and propane (C_3) concentrations measured with the headspace technique.

Table 13. Stratigraphic depths of the marker layers at Site 727 for layer-by-layer correlation to the Oman margin.

Layer	Hole 727A Core, section, interval (cm)	Hole 727A ODP depth (mbsf)	Hole 727B Core, section, interval (cm)	Hole 727B ODP depth (mbsf)	Holes 727B – 727A
OM-a_1			1H-2, 15	1.65	
a_2			1H-3, 55	3.55	
b_1	1H-3, 15	3.15	1H-5, 60	6.60	3.45
b_2	1H-4, 90	5.40	2H-1, 120	9.40	4.00
b_3	1H-5, 80	6.80	2H-2, 110	10.80	4.00
c_1	2H-1, 50	10.00	2H-5, 40	14.60	4.60
c_2	2H-2, 125	12.25	2H-6, 115	16.85	4.60
c_3	2H-3, 95	13.45			
c_4	2H-4, 30	14.30			
c_5	2H-4, 55	14.55			
d_1	2H-5, 100	16.50	3H-2, 35	19.45	2.95
d_2	2H-6, 15	17.15	3H-2, 100	20.10	2.95
d_3	2H-6, 110	18.10	3H-3, 55	21.15	3.05
d_4	3H-1, 90	19.80	3H-4, 75	22.85	3.05
e_1	3H-3, 5	21.95	3H-6, 5	25.15	3.25
e_2	3H-5, 25	25.15			
e_3	3H-5, 130	26.20			
f_1	3H-7, 25	28.15			
f_2	4H-2, 95	30.85			
g_1	4H-4, 100	33.90			
g_2	4H-7, 40	37.80			
h_1	5H-4, 40	42.70			
h_3	5H-6, 135	46.65			
h_4	6H-3, 95	51.25			
h_5	6H-4, 95	52.75			

Note: Depths are based on ODP CORELOG data

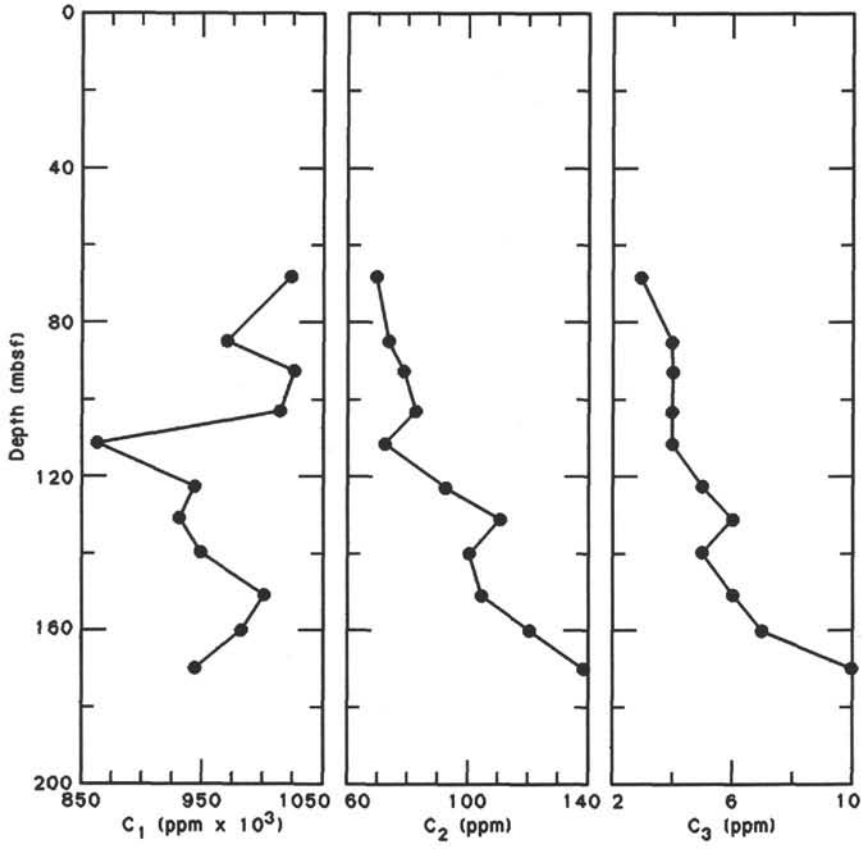

Figure 27. Downhole plot of methane (C_1), ethane (C_2), and propane (C_3) concentrations measured in vacutainer samples from gas pockets.

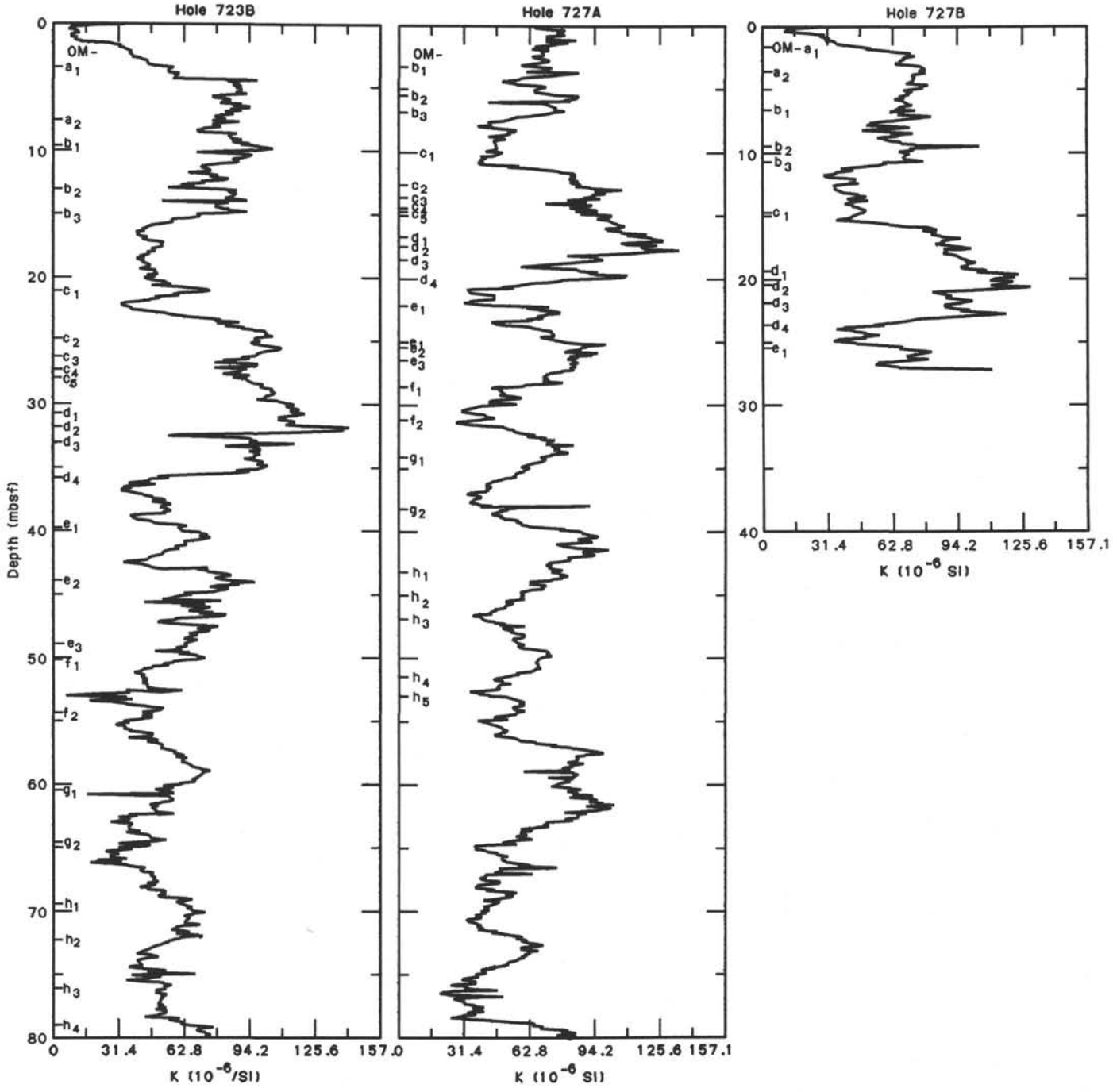

Figure 28. Magnetic susceptibility curve and positions of the marker layers in Holes 727A and 727B. Magnetic susceptibility curve and positions of the marker layers in Holes 723B and 727A. Note the similarity of the curves from these two different sites.

Table 14. Corrected sub-bottom depth of core-top for stratigraphic sub-bottom depth calculation.

	Hole 727A			Hole 727B		
Core	ODP top depth (mbsf)	Difference	Corrected top depth (mbsf)	ODP top depth (mbsf)	Difference	Corrected top depth (mbsf)
1H	0	3.4	3.4	0	0	0
2H	9.5	0.6	13.5	8.2	−0.6	7.6
3H	18.9	0.1	23.0	17.6	1.6	18.6
4H	28.4		32.5			
5H	37.8		41.9			
6H	47.3		51.4			

Note: ODP top depth = sub-bottom depth of core top calculated by the ODP CORELOG data. Difference = the difference between the depth calculated by the ODP CORELOG data and the depth calculated by the layer-by-layer correlation method. Corrected top depth = sub-bottom depth of core top calculated by the layer-by-layer correlation method.

Table 15. Stratigraphic depths of the marker layers at Sites 723, 724, and 727.

	Hole 723B		Hole 724A		Hole 727A		Hole 727B	
Layer	Core, section, interval (cm)	Corrected depth (mbsf)	Core, section, interval (cm)	Corrected depth (mbsf)	Core, section, interval (cm)	Corrected depth (mbsf)	Core, section, interval (cm)	Corrected depth (mbsf)
OM-a_1	1H-3, 35	3.35	1H-1, 95	0.95			1H-2, 15	1.65
a_2	2H-3, 20	7.20	1H-2, 115	2.65			1H-3, 55	3.55
b_1	2H-4, 65	9.15	1H-3, 100	4.00	1H-3, 15	6.55	1H-5, 60	6.60
b_2	2H-6, 110	12.60			1H-4, 90	8.80	2H-1, 120	8.80
b_3	3H-1, 95	14.75	2H-1, 40	7.60	1H-5, 80	10.20	2H-2, 110	10.20
c_1	3H-5, 110	20.90	2H-2, 75	9.45	2H-1, 50	14.00	2H-5, 40	14.00
c_2	4H-1, 85	24.95	2H-3, 130	11.50	2H-2, 125	16.25	2H-6, 115	16.25
c_3	4H-2, 100	26.60	2H-4, 70	12.40	2H-3, 95	17.45		
c_4	4H-3, 15	27.25	2H-4, 120	12.90	2H-4, 30	18.30		
c_5	4H-3, 100	28.10	2H-5, 35	13.55	2H-4, 55	18.55		
d_1	4H-5, 70	30.80	3H-1, 40	17.20	2H-5, 100	20.50	3H-2, 35	20.45
d_2	4H-6, 10	31.70	3H-1, 150	18.30	2H-6, 15	21.15	3H-2, 100	21.10
d_3	4H-7, 5	33.15	3H-2, 90	19.20	2H-6, 110	22.10	3H-3, 55	22.15
d_4	5H-2, 50	35.30	3H-3, 85	20.65	3H-1, 90	23.90	3H-4, 75	23.85
e_1	5H-5, 20	39.50	3H-4, 15	21.45	3H-3, 5	26.05	3H-6, 5	26.15
e_2	6H-1, 90	43.80	3H-5, 90	23.70	3H-5, 25	29.25		
e_3	6H-3, 150	47.40	3H-6, 95	25.25	3H-5, 130	30.30		
f_1	6H-5, 120	50.10	4H-1, 85	27.75	3H-7, 25	32.25		
f_2	7H-2, 15	54.25	4H-2, 70	29.10	4H-2, 95	34.95		
g_1	7H-6, 30	60.40	4H-4, 120	32.60	4H-4, 100	38.00		
g_2	8H-2, 60	64.40	4H-6, 25	34.65	4H-7, 40	41.90		
h_1	8H-5, 90	69.20	4H-7, 40	36.30	5H-4, 40	46.80		
h_2	9H-1, 20	72.10	5H-1, 80	37.30				
h_3	9H-3, 135	76.25	5H-2, 60	38.60	5H-6, 135	50.75		
h_4	9H-7, 95	81.85	5H-4, 145	42.45	6H-3, 95	55.35		
h_5			5H-5, 145	43.95	6H-4, 95	56.85		

Note: Depths based on the correction factors of Table 14.

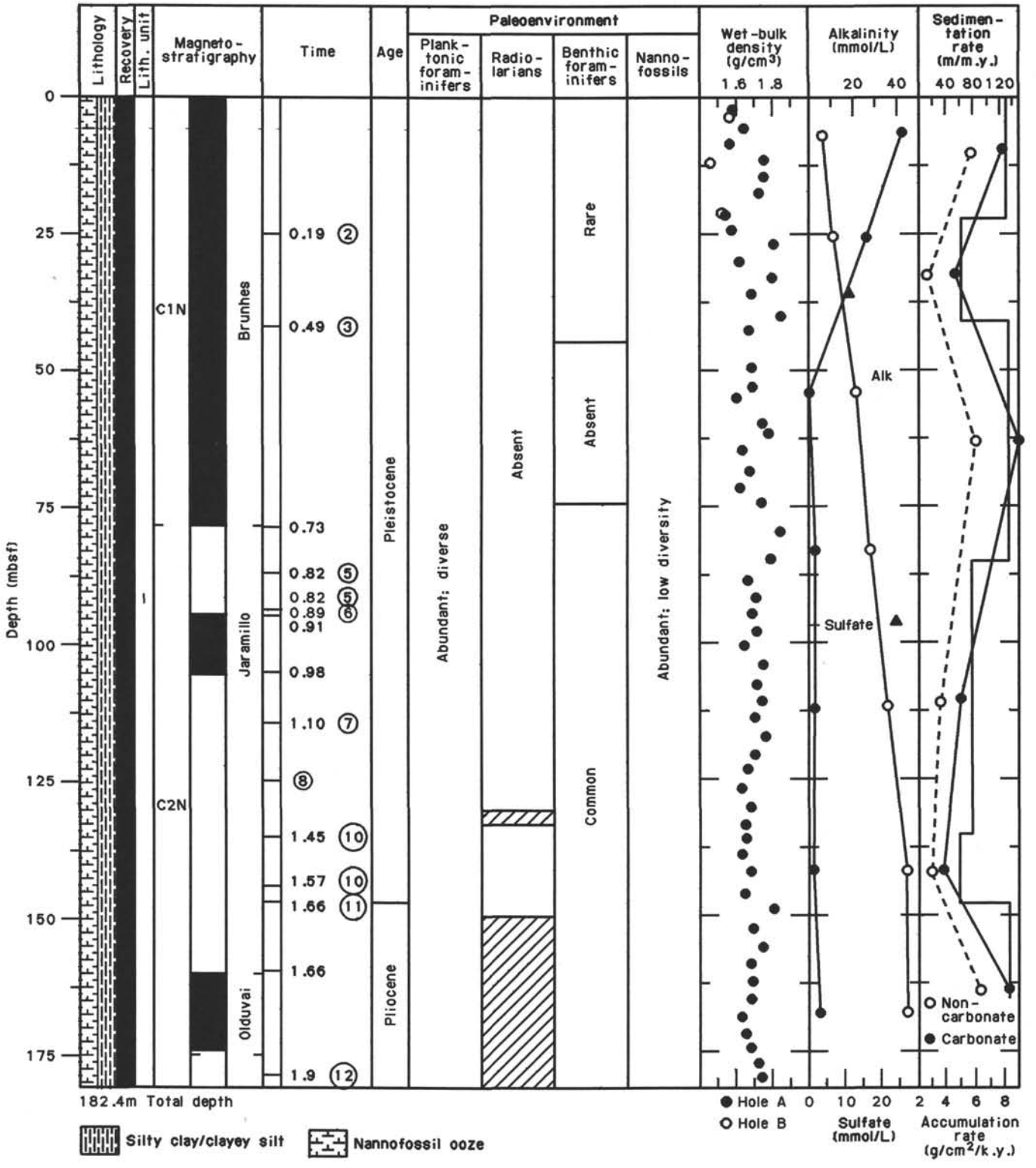

Figure 29. Summary chart of preliminary shipboard findings, Site 727.